IRAK1-dependent Regnase-1-14-3-3 complex formation controls Regnase-1-mediated mRNA decay

Kotaro Akaki[1,2], Kosuke Ogata[3], Yuhei Yamauchi[4], Noriki Iwai[1], Ka Man Tse[1], Fabian Hia[1], Atsushi Mochizuki[4], Yasushi Ishihama[3], Takashi Mino[1], and Osamu Takeuchi[1*]

[1]Department of Medical Chemistry, Graduate School of Medicine, Kyoto University, Kyoto 606-8501, Japan

[2]Graduate School of Biostudies, Kyoto University, Kyoto 606-8501, Japan

[3]Department of Molecular and Cellular BioAnalysis, Graduate School of Pharmaceutical Sciences, Kyoto University, Kyoto 606-8501, Japan

[4]Laboratory of Mathematical Biology, Institute for Frontier Life and Medical Sciences, Kyoto University, Kyoto 606-8507, Japan

*Correspondence: otake@mfour.med.kyoto-u.ac.jp (O.T.)

Abstract

Regnase-1 is an endoribonuclease crucial for controlling inflammation by degrading mRNAs encoding cytokines and inflammatory mediators in mammals. However, it is unclear how Regnase-1-mediated mRNA decay is controlled in interleukin (IL)-1β or Toll-like receptor (TLR) ligand-stimulated cells. Here, by analyzing the Regnase-1 interactome, we found that IL-1β or TLR stimulus dynamically induced the formation of Regnase-1-β-transducin repeat-containing protein (βTRCP) complex. Importantly, we also uncovered a novel interaction between Regnase-1 and 14-3-3 in both mouse and human cells. Strikingly, both interactions occur in a mutually exclusive manner, underscoring the importance of modulating Regnase-1's activity. Additionally, we show that in IL-1R/TLR-stimulated cells, the Regnase-1-14-3-3 interaction is mediated by IRAK1 through a previously uncharacterized C-terminal structural domain. Phosphorylation of Regnase-1 at S494 and S513 is critical for Regnase-1-14-3-3 interaction, while a different set of phosphorylation sites of Regnase-1 are known to be required for the recognition by βTRCP and proteasome-mediated degradation. 14-3-3 stabilizes Regnase-1 but abolishes its activity by inhibiting Regnase-1-mRNA association. Furthermore, nuclear-cytoplasmic shuttling of Regnase-1 is abrogated by 14-3-3 interaction. Taken together, the results suggest that a novel inflammation-induced interaction of 14-3-3 with Regnase-1 stabilizes inflammatory mRNAs by sequestering Regnase-1 in the cytoplasm to prevent mRNA recognition.

Introduction

The expression of proinflammatory cytokines is the hallmark of innate immune responses against microbial infection. Whereas inflammatory responses are critical for the elimination of invading pathogens, excess and chronic inflammation can culminate in tissue destruction and autoimmune diseases. When innate immune cells encounter pathogen-associated molecular patterns (PAMPs) or damage-associated molecular patterns (DAMPs), they are sensed by pattern-recognition receptors such as Toll-like receptors (TLRs), triggering the transcription of inflammatory genes (Fitzgerald & Kagan, 2020; Takeuchi & Akira, 2010).

The expression of inflammatory genes is also controlled by post-transcriptional mechanisms to facilitate or limit inflammatory responses (Anderson, 2010; Carpenter et al., 2014; Turner & DÍaz-Muñoz, 2018). Regnase-1 (also referred to as Zc3h12a or Mcpip1), an RNase, is a critical regulator of inflammation. Regnase-1 binds to and degrades inflammatory mRNAs such as *IL6* or *IL12b* by recognizing stem-loop structures present in the 3' untranslated regions (Matsushita et al., 2009; Mino et al., 2015). *Regnase-1*-deficient mice exhibit an autoimmune phenotype, indicating its importance as a negative regulator of inflammation (Matsushita et al., 2009; Uehata et al., 2013). Regnase-1 efficiently suppresses the expression of its target genes by degrading CBP80-bound mRNAs during the pioneer-round of translation by associating with ribosome and a helicase protein, UPF1 (Mino et al., 2015, 2019). CBP80 binds to newly synthesized mRNAs in the nucleus and is replaced by eIF4E after the pioneer round of translation following mRNA export from the nucleus (Maquat et al., 2010; Müller-Mcnicoll & Neugebauer, 2013). Thus, it is possible that

Regnase-1 recognizes target mRNAs in the steps leading to the pioneer round of translation.

The stability of cytokine mRNAs is dynamically regulated in innate immune cells under inflammatory conditions (Carpenter et al., 2014; Hao & Baltimore, 2009; Turner & DÍaz-Muñoz, 2018). Post-translational control of Regnase-1 in response to inflammatory stimuli contributes to extending half-lives of inflammatory mRNAs. Stimulation of cells with TLR-ligands, IL-1β, or IL-17 results in the activation of IκB kinases (IKKs), which phosphorylate Regnase-1 at S435 and S439, in addition to IκBα (Iwasaki et al., 2011; Kakiuchi et al., 2020; Nanki et al., 2020; Tanaka et al., 2019). Regnase-1, phosphorylated at S435 and S439 is subsequently recognized by βTRCP, one of the components in the SKP1-CUL1-F-box (SCF) complex, which induces K48-linked polyubiquitination of Regnase-1, followed by proteasome-mediated degradation (Iwasaki et al., 2011). On the other hand, these stimuli also induce transcription of *Regnase-1* (Iwasaki et al., 2011). Consequently, the protein level of Regnase-1 drastically changes during these stimulations; Regnase-1 levels decrease immediately after the stimulation and then increase to levels higher than its pre-stimulation. However, the post-translational regulatory mechanism of Regnase-1 following inflammatory stimuli is still not fully elucidated.

14-3-3 family proteins are conserved among species and are known to form hetero- or homo-dimer (Aitken, 2006; Pennington et al., 2018). The 14-3-3 dimer binds to various phosphorylated proteins using its two phosphor-S/T binding pockets which recognize unique phospho-peptides (Muslin et al., 1996; Yaffe et al., 1997). Although 14-3-3 itself has no enzymatic activity, 14-3-3 is known to modulate the properties of target proteins, such as

protein stability or localization (Aitken, 2006; Pennington et al., 2018).

In this study, we utilized an interactome-based approach to isolate Regnase-1 protein complexes and found that TLR-ligand, IL-1β, or IL-17 stimulation induces the formation of the Regnase-1-14-3-3 or -βTRCP complex in a mutually exclusive manner. The phosphorylation of Regnase-1 at S494 and S513 is responsible for binding with 14-3-3, which in turn stabilizes Regnase-1 protein by excluding βTRCP competitively. However, 14-3-3-bound Regnase-1 is not functional because 14-3-3 prevents Regnase-1 from recognizing target mRNAs. In addition, we found that nuclear-cytoplasmic shuttling of Regnase-1 is inhibited by 14-3-3's association with Regnase-1. Collectively, we identified a novel 14-3-3-mediated molecular mechanism which controls Regnase-1; a distinctly independent mechanism from βTRCP-mediated protein degradation of Regnase-1.

Results

Regnase-1 interactome analysis revealed dynamic recruitment of 14-3-3 upon stimulation

To comprehensively uncover Regnase-1-associating proteins in steady state and under inflammatory conditions, we stimulated HeLa cells expressing FLAG-HA-tagged Regnase-1 with or without IL-1β and immunoprecipitated Regnase-1 immediately after treatment with a crosslinking reagent, Dithiobis(succinimidyl propionate) (DSP) (Figure 1A). Consistent with previous reports, mass spectrometry analysis revealed that Regnase-1 interacted with translation-related proteins such as ribosomal proteins in unstimulated cells (Mino et al., 2015). Whereas IL-1β stimulation reduced the association between Regnase-1 and translation-related proteins, the stimulation strongly induced the association between Regnase-1 and SCF complex proteins such as βTRCP1/2, CUL1, and SKP1 (Iwasaki et al., 2011). In addition to these proteins, we identified 14-3-3 family proteins as novel Regnase-1-associating proteins under IL-1β-stimulated conditions (Figure 1B). Consistently, immunoprecipitation analysis revealed that endogenous Regnase-1 was co-precipitated with Myc-tagged 14-3-3ε as well as with HA-tagged βTRCP in HeLa cells in response to IL-1β stimulation (Figure 1C).

As the 14-3-3 family consists of seven paralogs in human and mouse (Aitken, 2006), we investigated the binding of these members to Regnase-1 via immunoprecipitation (Figure 1—figure supplement 1). Among seven of the 14-3-3 proteins, 14-3-3-β, γ, and ε strongly interacted with Regnase-1, while 14-3-3-ζ, η, and θ showed weak interaction. Interestingly,

Regnase-1 failed to associate with 14-3-3-σ, the latter of which was reported to exclusively form a homodimer but not a heterodimer with other 14-3-3 isoforms (Verdoodt et al., 2006).

To investigate if stimulation with TLR ligands also induces Regnase-1-14-3-3 binding, we stimulated RAW267.4 macrophages stably expressing Myc-14-3-3ε with Pam_3CSK_4 (a ligand for TLR1/2), poly I:C (a ligand for TLR3), LPS (a ligand for TLR4), R848 (a ligand for TLR7/8), or CpG DNA (a ligand for TLR9), and immunoprecipitated 14-3-3ε with an anti-Myc antibody. The Regnase-1-14-3-3 interaction was induced by all TLR ligands tested except for poly I:C (Figure 1D). All TLRs other than TLR3 signal through MyD88, while TLR3 utilizes TRIF as an adaptor to trigger intracellular signaling (Fitzgerald & Kagan, 2020; O'Neill et al., 2013; Takeuchi & Akira, 2010). Considering that IL-1β signal is also dependent on MyD88 (Akira et al., 2006), MyD88-dependent, but not TRIF-dependent, signaling pathways trigger the Regnase-1-14-3-3 binding.

Collectively, these results demonstrate that IL-1R/TLR stimulation induces dynamic remodeling of the Regnase-1-associating protein complex from translation machineries to SCF complexes and/or 14-3-3 proteins.

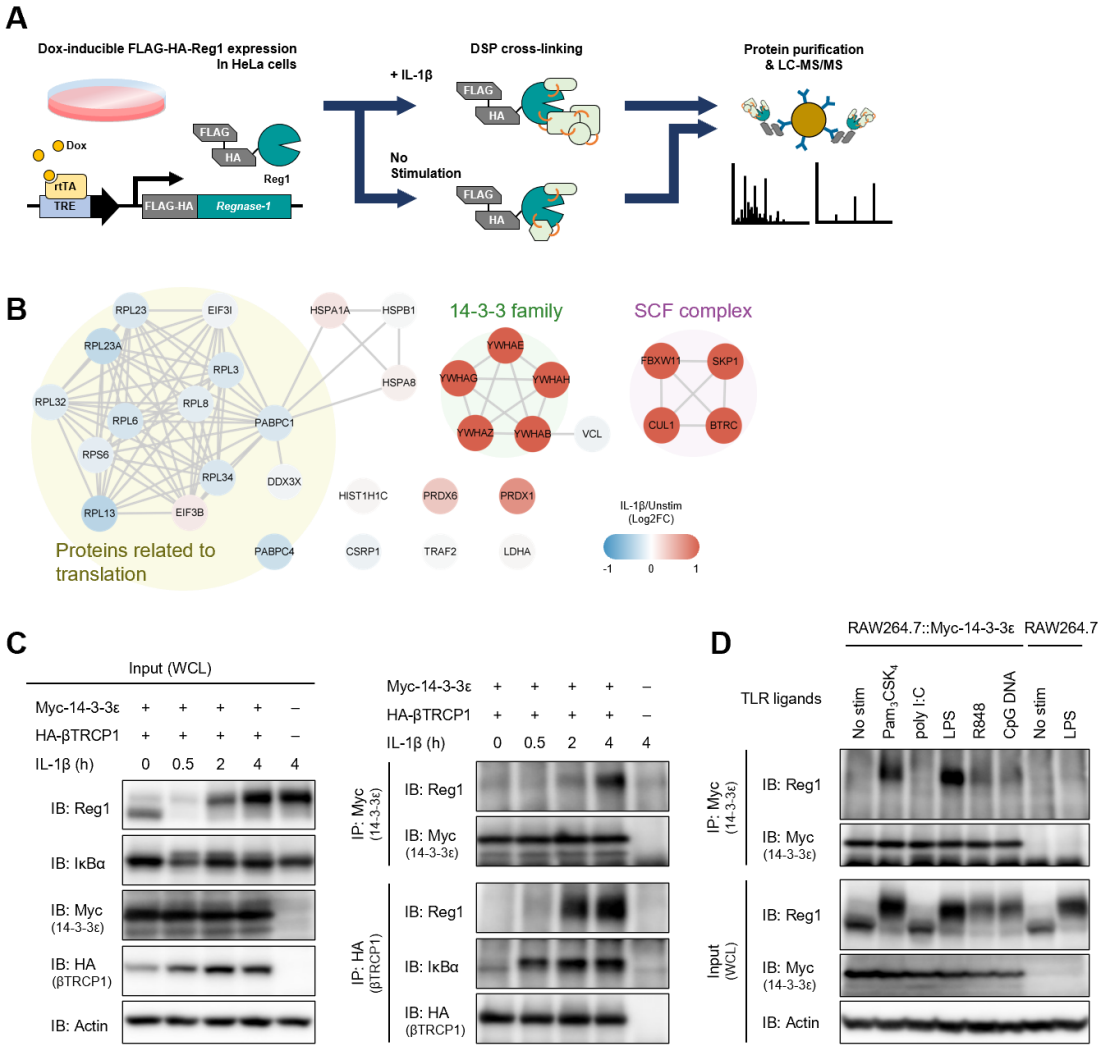

Figure 1 | IL-1β or TLR1/2/4/7/8/9-ligand stimulation induces Regnase-1-14-3-3 interaction.

(**A**) Schematic illustration of the DSP-crosslinking workflow. (**B**) Protein-protein interaction of the Regnase-1 (Reg1)-associating proteins. Each node represents Regnase-1 associating protein. The proteins whose association with Regnase-1 is weakened or enhanced in IL-1β-

stimulated cells are colored in blue or red, respectively. (**C**) Immunoblot analysis of immunoprecipitates (IP: Myc or IP: HA) and WCL (whole cell lysates) from HeLa cells transiently expressing Myc-14-3-3ε and HA-βTRCP1 stimulated with IL-1β (10 ng/ml) for indicated time. (**D**) Immunoblot analysis of immunoprecipitates (IP: Myc) and WCL from RAW264.7 or RAW264.7 stably expressing Myc-14-3-3ε stimulated with Pam_3CSK_4 (10 ng/ml), poly I:C (100 μg/ml), LPS (100 ng/ml), R848 (100 nM), or CpG DNA (1 μM) for 4 hours.

Phosphorylation of Regnase-1 at S494 and S513 is necessary for Regnase-1-14-3-3 binding

Since 14-3-3 proteins are known to recognize phosphorylated proteins (Muslin et al., 1996), we investigated if 14-3-3-bound Regnase-1 is phosphorylated by inflammatory stimuli. SDS-PAGE analysis revealed that Regnase-1 band migration was slower in samples stimulated with IL-1β or TLR ligands - a hallmark of Regnase-1 phosphorylation (Figure 1C–D, 2A, and Figure 2—figure supplement 1) (Iwasaki et al., 2011; Tanaka et al., 2019). Indeed, the mobility change of Regnase-1 was abolished when the cell lysates were treated with λ-protein phosphatase (λPP) (Figure 2A–B). Furthermore, the Regnase-1 band in the 14-3-3-precipitate migrated slower; λPP treatment of the 14-3-3-precipitate abolished this phenomenon (Figure 2A–B). Thus, 14-3-3 specifically binds to phosphorylated Regnase-1.

We next scrutinized Regnase-1 phosphorylation sites induced by IL-1β stimulation to identify phosphorylation sites critical for the Regnase-1-14-3-3 interaction. We purified

FLAG-HA-Regnase-1 from HeLa cells stimulated with or without IL-1β and identified IL-1β-inducible phosphorylation sites by LC-MS/MS (Figure 2C and Figure 2—figure supplement 1). We found that the phosphorylation at S21, S61, S62, S362, S439, S470, S494, and S513 of Regnase-1 was increased in response to IL-1β stimulation. To identify Regnase-1 phosphorylation sites responsible for binding with 14-3-3, we mutated serine residues on Regnase-1 phosphorylation sites into alanine and probed its association with 14-3-3. Among the Regnase-1-SA mutants, S494A and S513A mutants failed to be co-precipitated with 14-3-3 (Figure 2D), indicating that phosphorylation at both of S494 and S513 is necessary for the Regnase-1-14-3-3 interaction. Both phosphorylation sites harbor a pSxP sequence, which shows similarity with a known 14-3-3 binding motif, RxxpSxP, mode 1 (Yaffe et al., 1997). Noteworthy, amino acid sequences surrounding S494 and S513 are highly conserved among many species (Figure 2E–F).

We next investigated the mechanism of how Regnase-1 phosphorylation is regulated by inflammatory stimuli. In response to IL-1β or TLR ligands stimulation, MyD88 associates with IRAK kinases, IRAK1 and IRAK2, via the death domain (Gottipati et al., 2008; Wesche et al., 1997). A part of C-terminal region of IRAKs in turn interacts with TRAF6 to activate NF-κB (Ye et al., 2002). We found that overexpression of IRAK1 and IRAK2 induced Regnase-1-14-3-3 binding (Figure 2G). In contrast, the interaction between Regnase-1 and 14-3-3 was not induced by the expression of a kinase-inactive mutant (T209A) IRAK1 (Kollewe et al., 2004) or a deletion mutant lacking death domain (Δ1-103) of IRAK1, indicating that the Regnase-1-14-3-3 binding requires the IRAK1 kinase activity as well as

recruitment to MyD88 (Figure 2H–I). Although the C-terminal 619-710 portion of IRAK1 was also required for Regnase-1-14-3-3 binding, point mutations in TRAF6 binding sites (E541/E584/E704A) (Ye et al., 2002) did not abolish the Regnase-1-14-3-3 binding (Figure 2H–I). *In silico* prediction suggested the presence of a C-terminal structural domain (CSD) in the 619-710 of IRAK1 (Figure 2—figure supplement 3). In the CSD of IRAK1, highly conserved amino acids, R663 and K665, are critical for the Regnase-1-14-3-3 binding (Figure 2I), suggesting that the CSD of IRAK1 controls Reganse-1-14-3-3 interaction irrespective of the recruitment of TRAF6. Of note, the R663/K665A mutant IRAK1 was capable of activating NF-κB (Figure 2—figure supplement 4), indicating that the IRAK1 C-terminal region has two distinct functions: NF-κB activation through TRAF6 binding sites and the induction of Regnase-1-14-3-3 interaction through the CSD.

S494 and S513 of Regnase-1 are also reported to be phosphorylated by overexpression of Act1 together with TANK-binding kinase 1 (TBK1) or IKK-i/ε, which mimics IL-17 signaling (Tanaka et al., 2019). We detected phosphorylation at S494 and S513 of Regnase-1 in IL-17A-stimulated cells as well as IL-1β-stimulated cells by LC-MS/MS (Figure 2—figure supplement 5, 6). Furthermore, we found that IL-17A stimulation also induced Regnase-1-14-3-3 binding (Figure 2—figure supplement 7).

Collectively, these data demonstrate that the IRAK-dependent phosphorylation of Regnase-1 at S494 and S513 is necessary for the association between Regnase-1 and 14-3-3.

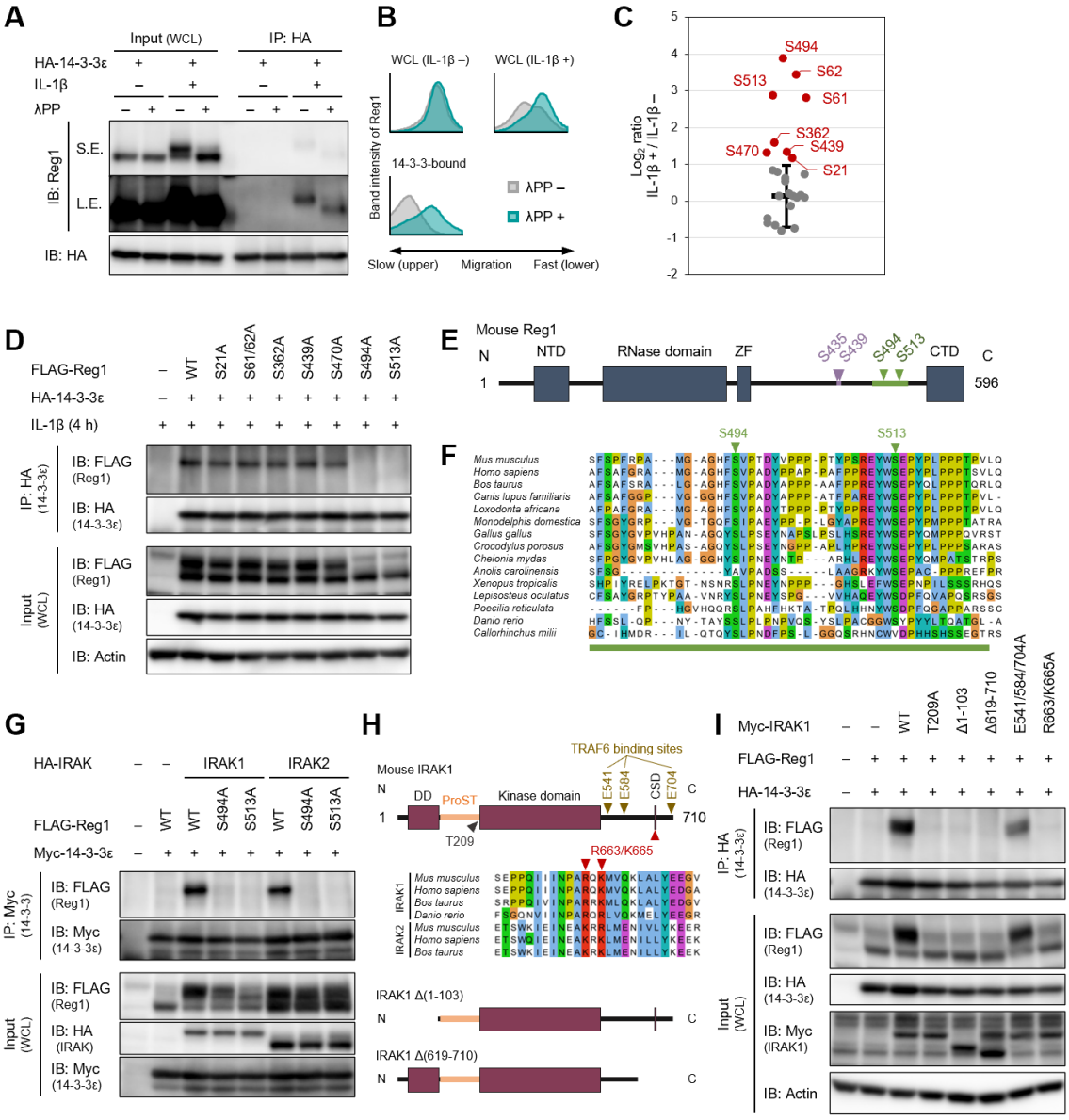

Figure 2 | IL-1β-induced phosphorylation of Regnase-1 at S494 and S513 is necessary for Regnase-1-14-3-3 binding.

(**A**) Immunoblot analysis of λPP-treated immunoprecipitates (IP: HA) and WCL from HeLa

cells transiently expressing HA-14-3-3ε stimulated with IL-1β (10 ng/ml) for 4 hours. S.E.: short exposure, L.E.: long exposure. (**B**) The intensity of Regnase-1-bands in (A). (**C**) Quantitation of phosphosites on Regnase-1 in HeLa cells stimulated with or without IL-1β (10 ng/ml) for 4 hours. Each dot shows phosphosite quantitative ratio between IL-1β + and IL-1β -. Phosphosites with $\log_2$ ratio > 1 were colored with red. Black horizontal line shows Regnase-1 protein quantitative ratio derived from the average of non-phosphopeptide quantitative ratios, and its error bars show the standard deviation. (**D**) Immunoblot analysis of immunoprecipitates (IP: HA) and WCL from HeLa cells transiently expressing HA-14-3-3ε and FLAG-Regnase-1-WT or indicated mutants stimulated with IL-1β for 4 hours. (**E**) Schematic illustration of Regnase-1 protein. The amino acid sequence including S494 and S513 shown in (E) is highlighted in green. NTD: N-terminal domain, ZF: Zinc finger domain, CTD: C-terminal domain. (**F**) The amino acid sequences including S494 and S513 of Regnase-1 from mouse and other indicated vertebrates. (**G**) Immunoblot analysis of immunoprecipitates (IP: Myc) and WCL from HeLa cells transiently expressing Myc-14-3-3ε and HA-Regnase-1-WT or indicated mutants stimulated with IL-1β (10 ng/ml) for 4 hours. (**H**) Schematic illustration of IRAK1 protein. The amino acid sequence in CSD of IRAK1 and IRAK2 from mouse and other indicated vertebrates are also shown. DD: Death domain, CSD: C-terminal structural domain. (**I**) Immunoblot analysis of immunoprecipitates (IP: HA) and WCL from HeLa cells transiently expressing FLAG-Regnase-1-WT, HA-14-3-3ε, and Myc-IRAK1-WT or indicated mutants.

181

The binding of 14-3-3 and βTRCP to Regnase-1 is mutually exclusive

MyD88-dependent signaling also induces IKK-mediated phosphorylation of Regnase-1 at S435 and S439, which allows recognition of Regnase-1 by βTRCP (Iwasaki et al., 2011). With this, we examined the relationship between the association of Regnase-1 to 14-3-3 and to βTRCP. We found that Regnase-1 harboring S435A and S439A mutations permitted interaction with 14-3-3 but failed to recruit βTRCP (Figure 3A–B). Reciprocally, the S494A or S513A mutation of Regnase-1 did not inhibit the association between Regnase-1 and βTRCP (Figure 2B), indicating that the phosphorylation of Regnase-1 at S494 or S513 or the Regnase-1-14-3-3 binding is dispensable for the Regnase-1-βTRCP association. We next checked the phosphorylation status of βTRCP-bound and 14-3-3-bound Regnase-1. Since βTRCP-mediated polyubiquitination potentially alters the molecular weight of Regnase-1, we utilized a βTRCP mutant which is unable to induce polyubiquitination due to the lack of the F-box domain (βTRCP-ΔF). Interestingly, the SDS-PAGE analysis revealed that βTRCP-ΔF-bound Regnase-1 migrated faster than 14-3-3-bound Regnase-1 (Figure 2C–D), indicating that βTRCP likely binds to 14-3-3-free Regnase-1.

These results demonstrate that the binding of Regnase-1 to 14-3-3 and βTRCP is a mutually exclusive event, although IL-1β stimulation simultaneously induces phosphorylation of Regnase-1 at S494 and S513 as well as S435 and S439.

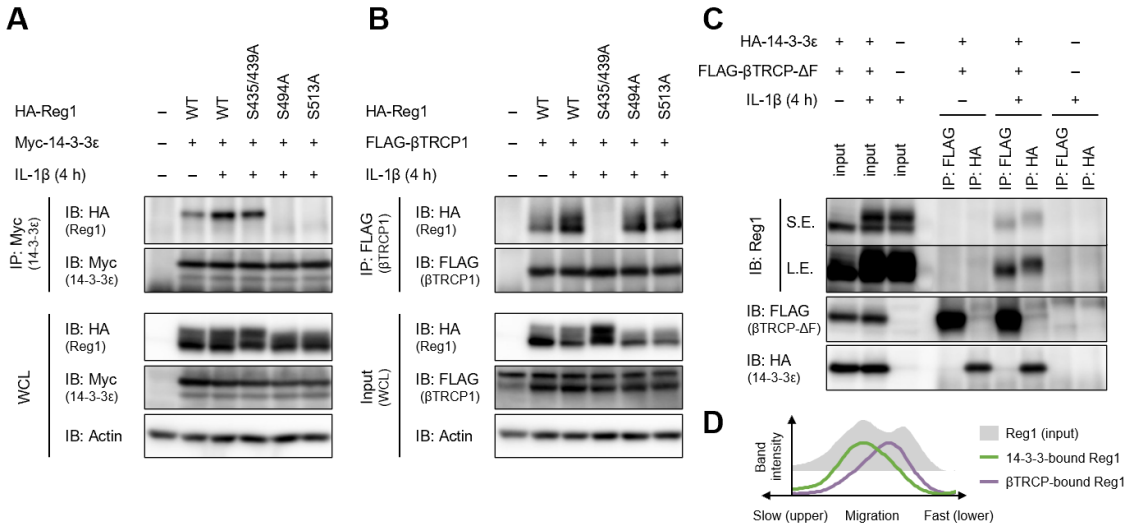

Figure 3 | The binding of 14-3-3 and βTRCP to Regnase-1 is mutually exclusive.

(**A**) Immunoblot analysis of immunoprecipitates (IP: Myc) and WCL from HeLa cells transiently expressing Myc-14-3-3ε and HA-Regnase-1-WT or indicated mutant stimulated with IL-1β (10 ng/ml) for 4 hours. (**B**) Immunoblot analysis of immunoprecipitates (IP: FLAG) and WCL from HeLa cells transiently expressing FLAG-βTRCP1 and HA-Regnase-1-WT or indicated mutant stimulated with IL-1β (10 ng/ml) for 4 hours. (**C**) Immunoblot analysis of immunoprecipitates (IP: FLAG or HA) and WCL from HeLa cells transiently expressing FLAG-βTRCP-ΔF and HA-14-3-3ε stimulated with IL-1β (10 ng/ml) for 4 hours. S.E.: short exposure, L.E.: long exposure. (**D**) The intensity of Regnase-1-bands in (C).

200

201 **The S513A mutation destabilizes Regnase-1 protein without affecting target mRNA**

202 **abundance**

203 To evaluate the functional roles of Regnase-1-14-3-3 interaction, we generated *Regnase-*

204 *1*$^{S513A/S513A}$ knock-in mice (Figure 4—figure supplement 1). *Regnase-1*$^{S513A/S513A}$ mice did
205 not show gross abnormality, nor did they exhibit alteration in the numbers of T, B cells or
206 macrophages (data not shown). We stimulated mouse embryonic fibroblasts (MEFs) derived
207 from *Regnase-1*$^{WT/WT}$ and *Regnase-1*$^{S513A/S513A}$ mice with IL-1β and checked Regnase-1
208 expression (Figure 4A). Immunoblot analysis revealed that Regnase-1 was degraded 30 min
209 after stimulation in both WT and S513A mutant MEFs. Following this, Regnase-1 levels
210 increased in WT MEFs at 2 and 4 hours after stimulation (Figure 4A). Notably, most of the
211 newly synthesized Regnase-1 showed slow migration and was able to associate with 14-3-3.
212 On the other hand, the slowly migrating Regnase-1 band did not appear in *Regnase-*
213 *1*$^{S513A/S513A}$ MEFs after IL-1β stimulation. Interestingly, the amount of Regnase-1 not
214 interacting with 14-3-3 (lower bands) was comparable between WT and *Regnase-1*$^{S513A/S513A}$
215 at corresponding time points. Consequently, total Regnase-1 protein expression was severely
216 reduced in *Regnase-1*$^{S513A/S513A}$ MEFs compared with WT after IL-1β stimulation (Figure
217 4A). Similar results were also obtained when bone marrow-derived macrophages (BMDMs)
218 and thioglycollate-elicited peritoneal exudate cells (PECs) derived from *Regnase-1*$^{WT/WT}$ and
219 *Regnase-1*$^{S513A/S513A}$ mice were stimulated with LPS (Figure 4B–C). Nevertheless, *Regnase-*
220 *1* mRNA levels were comparable between *Regnase-1*$^{WT/WT}$ and *Regnase-1*$^{S513A/S513A}$ cells
221 (Figure 4D–F), suggesting that S513A mutation affects protein stability of Regnase-1. Indeed,
222 treatment of *Regnase-1*$^{S513A/S513A}$ PECs with MG-132, a proteasome inhibitor, resulted in the
223 increase of smearing in the band patterns of Regnase-1 in LPS-stimulated cells (Figure 4C),
224 possibly due to the inhibition of degradation of polyubiquitinated Regnase-1. These data

indicate that the phosphorylation of Regnase-1 at S513 stabilizes Regnase-1 protein after IL-1β or LPS stimulation by binding with 14-3-3.

We next checked whether the altered Regnase-1 expression by the S513A mutation affects Regnase-1-mediated mRNA decay. Despite the huge difference in Regnase-1 expression, the expression of *Il6*, a transcript degraded by Regnase-1 (Figure 4—figure supplement 2), was comparable between *Regnase-1*$^{WT/WT}$ and *Regnase-1*$^{S513A/S513A}$ cells (Figure 3D–I). Even when we analyzed gene expression profile comparing *Regnase-1*$^{WT/WT}$ and *Regnase-1*$^{S513A/S513A}$ macrophages by an RNA-seq analysis (Figure 4—figure supplement 3), we did not identify any differentially expressed genes (adj $P<0.05$) between *Regnase-1*$^{WT/WT}$ and *Regnase-1*$^{S513A/S513A}$ macrophages irrespective of the stimulation with LPS.

To examine the mechanisms underlying these observations, we developed two mathematical models based on our previous studies (see Materials and Methods) (Iwasaki et al., 2011; Mino et al., 2019). The first model (Model 1) assumes that 14-3-3-bound Regnase-1 is unable to degrade its target mRNAs (Figure 4J). The second model (Model 2) assumes that Regnase-1 binding with 14-3-3 maintains its ability to degrade its target mRNAs to a certain extent (Figure 4K). Mathematical analysis showed that in Model 2, the abundance of the *Il6* mRNAs should be different between *Regnase-1*$^{WT/WT}$ and *Regnase-1*$^{S513A/S513A}$ cells under the condition that the amount of 14-3-3-free Regnase-1 protein (lower bands in Figure 4A–C) is comparable between them. Our observations that the abundance of the target mRNAs did not differ between *Regnase-1*$^{WT/WT}$ and *Regnase-1*$^{S513A/S513A}$ cells in the late

246 phase of stimulation is inconsistent with Model 2, suggesting that Reganse-1 is inactivated
247 upon binding to 14-3-3.

248 These results suggest that the phosphorylation at S513 and the following association
249 with 14-3-3 nullifies Regnase-1's ability in degrading target mRNAs, although it stabilizes
250 and significantly upregulates the abundance of Regnase-1.

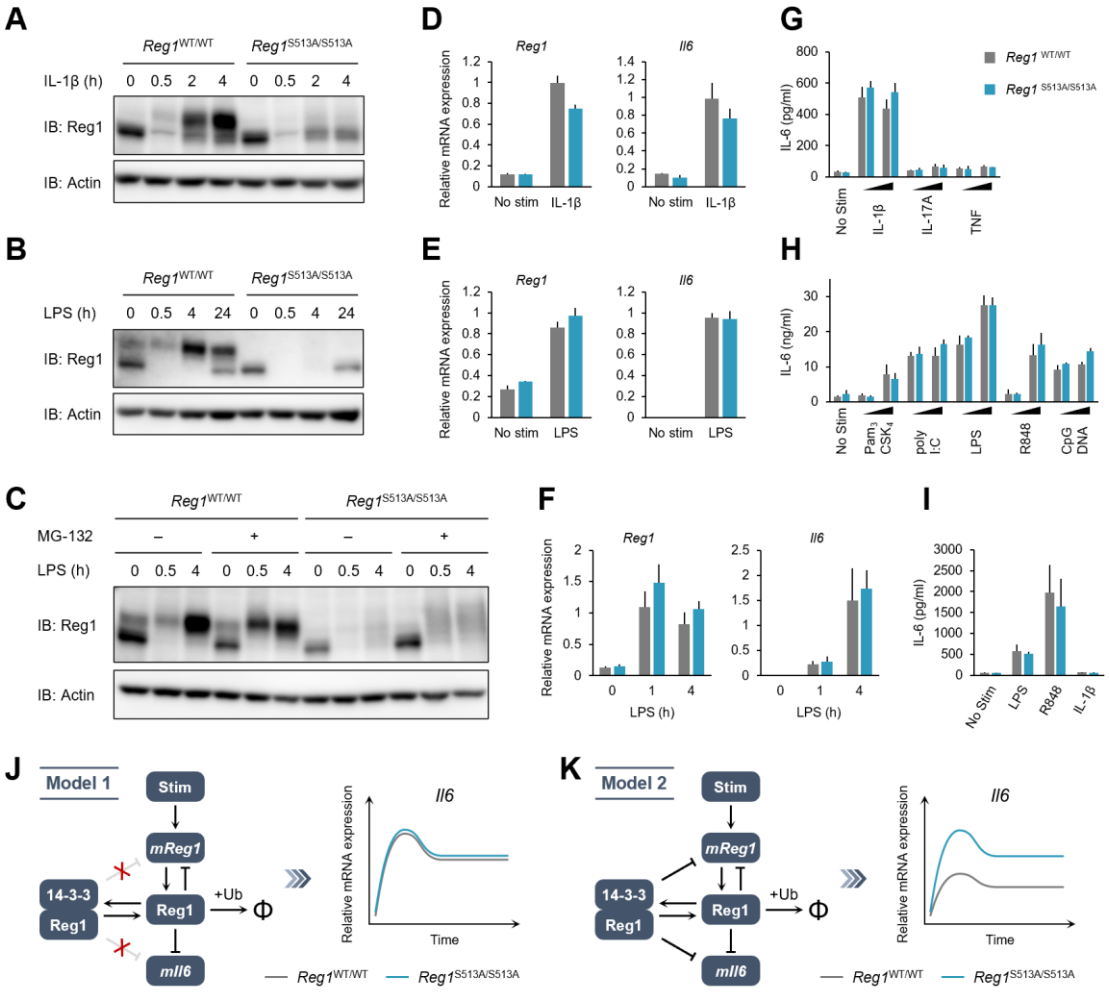

Figure 4 | The S513A mutation destabilizes Regnase-1 protein but does not affect target mRNA abundance.

(**A**)-(**C**) Immunoblot analysis of *Regnase-1*$^{WT/WT}$ and *Regnase-1*$^{S513A/S513A}$ MEFs stimulated with IL-1β (10 ng/ml) (A), BMDMs stimulated with LPS (100 ng/ml) (B), and thioglycollate-elicited PECs stimulated with LPS (100 ng/ml) (C) for indicated time. PECs were pretreated with MG-132 (5 μM) 2 hours before the stimulation. (**D**)-(**F**) mRNA expression of *Regnase-*

1 and *Il6* in *Regnase-1*$^{WT/WT}$ and *Regnase-1*$^{S513A/S513A}$ MEFs stimulated with IL-1β (10 ng/ml) for 4 hours (D), BMDMs stimulated with LPS (100 ng/ml) for 4 hours (E), and thioglycollate-elicited PECs stimulated with LPS (100 ng/ml) for indicated time (F). (**G**)-(**I**) IL-6 secretion in *Regnase-1*$^{WT/WT}$ and *Regnase-1*$^{S513A/S513A}$ MEFs stimulated with IL-1β (10 ng/ml), IL-17A (50 ng/ml), or TNF (10 ng/ml) for 24 hours (G), BMDMs stimulated with Pam_3CSK_4 (1 or 10 ng/ml), poly I:C (10 or 100 ng/ml), LPS (10 or 100 ng/ml), R848 (10 or 100 nM), or CpG DNA (0.1 or 1 μM) for 24 hours (H), and thioglycollate-elicited PECs stimulated with LPS (100 ng/ml), R848 (100 nM), or IL-1β (10 ng/ml) for 24 hours (I). (**J**) Schematic representation of Model 1 in which 14-3-3-bound Reganse-1 does not have the function of degrading its target mRNAs This model could explain the experimental observations. (**K**) Schematic representation of Model 2 in which 14-3-3-bound Reganse-1 maintains some ability to degrade its target mRNAs This model is not consistent with the experimental observations.

In (D)-(I), bars represent mean values of biological replicates ($n = 3$), and error bars represent standard deviation. Similar results were obtained from at least two independent experiments.

14-3-3 inactivates Regnase-1 by inhibiting Regnase-1-RNA binding

The mathematical analysis suggests that 14-3-3-bound Regnase-1 is inactive as the S513A mutation failed to affect *Il6* expression in MEFs or macrophages. To examine if this comparable *Il6* expression was due to increased degradation of Regnase-1-S513A protein via βTRCP, we further mutated βTRCP-recognition sites, S435 and S439, to alanine in Regnase-

1-S513A (Regnase-1-S435/439/513A). As shown in Figure 5A, Regnase-1-S435/439/513A was more potent in suppressing *Il6* expression compared to WT or other SA mutants, S435/439A and S513A, in response to IL-1β stimulation. These results indicate that IL-1β stimulation regulates Regnase-1 by two independent mechanisms via 14-3-3 and βTRCP, respectively.

To further examine the mechanism of how 14-3-3 inactivates Regnase-1, we attempted to generate a Regnase-1 mutant which constitutively binds to 14-3-3 even without stimulation. We generated a phospho-mimic mutant of Regnase-1 (S494D/S513D). However, this mutant failed to bind 14-3-3 (Figure 5B), indicating that the phosphate moiety, but not negative charge, is recognized by 14-3-3. Then we utilized a sequence of Exoenzyme S (ExoS), which is a bacterial protein derived from *Pseudomonas aeruginosa* and is known to bind to 14-3-3 without phosphorylation (Fu et al., 1993; Karlberg et al., 2018; Masters et al., 1999). The 22 amino acids of Regnase-1 covering S494 and S513 were substituted with two ExoS (419-429) sequences (Figure 5C). As a control, we additionally mutated Regnase-1-ExoSx2 by substituting its core sequences for 14-3-3 binding (L426, D427, and L428) with alanine residues (Regnase-1-ExoSAAAx2) (Ottmann et al., 2007; Yasmin et al., 2006). We observed that Regnase-1-ExoSx2, but not Regnase-1-ExoSAAAx2, interacted with endogenous 14-3-3 without any stimulation (Figure 5B). Using these mutants, we investigated whether 14-3-3 binding alters the activity of Regnase-1 to suppress *Il6* expression. Consistent with its 14-3-3 binding capacity, Regnase-1-ExoSx2, but not Regnase-1-ExoSAAAx2 and -S494D/S513D, lost the activity to inhibit *Il6* expression

(Figure 5D). Furthermore, the production of IL-6 protein was similarly inhibited depending on the capacity of Regnase-1 to bind 14-3-3 (Figure 5E). In addition, Regnase-1-mediated suppression of *Il6* expression was impaired by the overexpression of IRAK1-WT and E541/E584/E704A mutants, both of which induce Regnase-1-14-3-3 association (Figure 5F). On the other hand, IRAK1 mutants that failed to induce Regnase-1-14-3-3 association (T209A, Δ1-103, Δ619-710, and R663/K665A) did not affect the activity of Regnase-1.

We next examined how 14-3-3 inhibits the activity of Regnase-1 by investigating Regnase-1-mRNA binding activity using various Regnase-1 mutants. To stabilize Regnase-1-RNA binding, we generated a nuclease inactive version of Regnase-1 by introducing the D141N mutation to each of Regnase-1 mutant (Matsushita et al., 2009) (Figure 5—figure supplement 1). As shown in Figure 5G, forced interaction of Regnase-1-D141N with 14-3-3 by the ExoSx2 mutation abrogated the binding with *IL6* mRNA, whereas *IL6* was co-precipitated with Regnase-1-D141N, -ExoSAAAx2-D141N and -S494D/S513D-D141N (Figure 5G). Collectively, these data demonstrate that 14-3-3 inhibits Regnase-1-mRNA binding, thereby abrogating Regnase-1-mediated mRNA degradation.

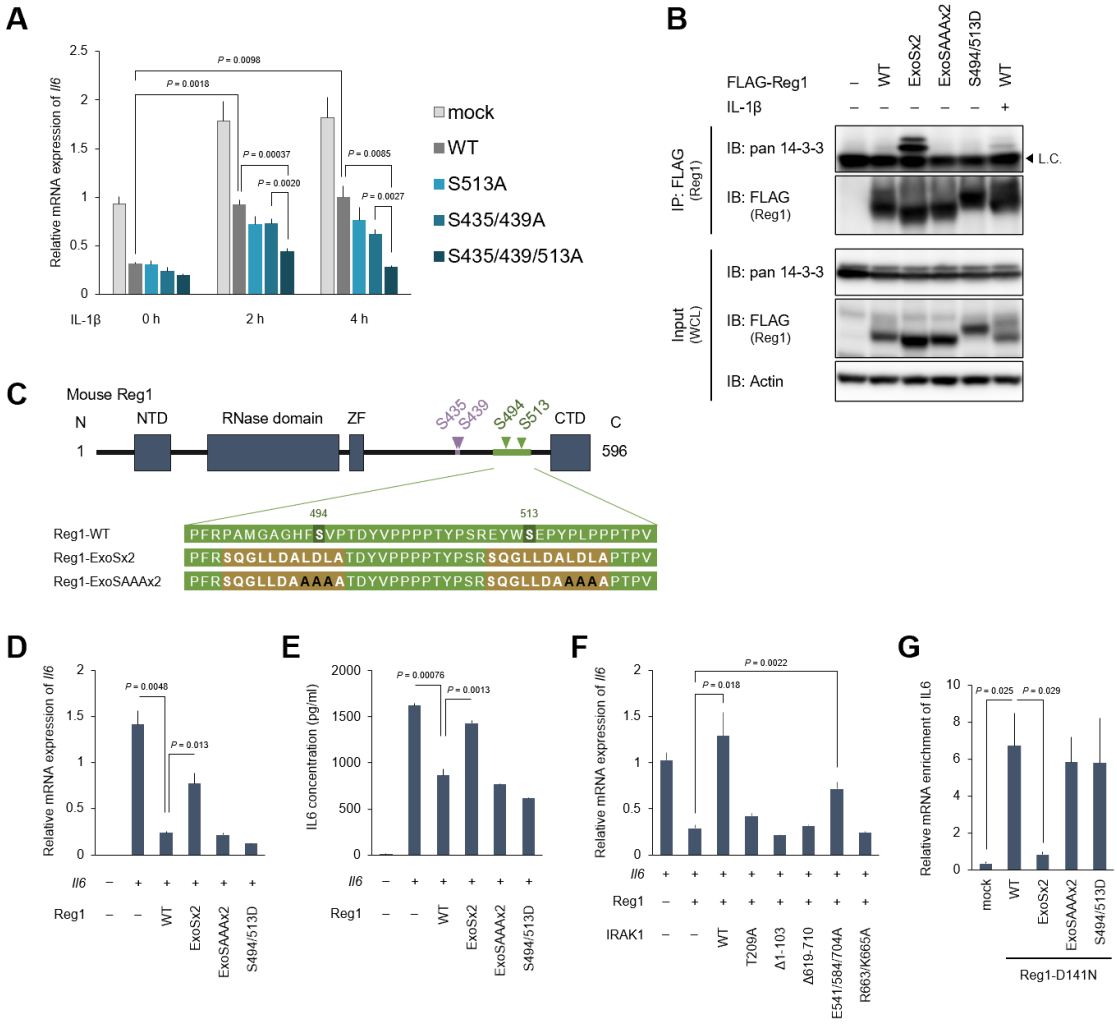

Figure 5 | 14-3-3 bound to phospho-S494 and S513 inactivates Regnase-1 by inhibiting Regnase-1-mRNA binding.

(**A**) mRNA expression of *Il6* in HeLa cells transiently expressing Regnase-1-WT or indicated mutants together with Il6. Cells were stimulated with IL-1β (10 ng/ml) for indicated time. (**B**) Immunoblot analysis of immunoprecipitates (IP: FLAG) and WCL from HeLa cells transiently expressing FLAG-Regnase-1-WT or indicated mutants. For the IL-1β stimulation,

cells were stimulated with IL-1β (10 ng/ml) for 4 hours. L.C.: light chain. (**C**) Schematic illustration of Regnase-1 and the amino acid sequences of Regnase-1-WT, -ExoSx2, and ExoSAAAx2. NTD: N-terminal domain, ZF: Zinc finger domain, CTD: C-terminal domain. (**D**) mRNA expression of *Il6* in HeLa cells transiently expressing Regnase-1-WT or indicated mutants together with Il6. (**E**) Secreted IL6 concentration in (D). (**F**) mRNA expression of *Il6* in HeLa cells transiently expressing Regnase-1-WT and IRAK1-WT or indicated mutants together with *Il6*. (**G**) The amount of *IL6* mRNAs immunoprecipitated with FLAG-Regnase-1-D141N or other indicated mutants in HeLa cells.

In (A), (D)-(G), bars represent mean values of biological replicates (n = 3), and error bars represent standard deviation. P-values were calculated using unpaired, two-sided t-test. Similar results were obtained from at least two independent experiments.

14-3-3 inhibits nuclear import of Regnase-1

We have previously shown that Regnase-1 interacts with CBP80-bound, but not eIF4E-bound, mRNAs (Mino et al., 2019), indicating that Regnase-1 degrades mRNAs immediately after the export from the nucleus to the cytoplasm (Maquat et al., 2010; Müller-Mcnicoll & Neugebauer, 2013). Although Regnase-1 mainly localizes in the cytoplasm (Mino et al., 2015), we hypothesized Regnase-1 shuttles between the nucleus and the cytoplasm to recognize its target mRNAs in association with their nuclear export. To test this hypothesis, we examined the subcellular localization of Regnase-1 following the treatment with Leptomycin B (LMB), which inhibits CRM1 (also known as Exportin-1)-mediated protein

303 export from the nucleus to the cytoplasm (Yashiroda & Yoshida, 2005). Whereas Regnase-1
304 localized in the cytoplasm in the steady state condition, LMB treatment induced rapid
305 accumulation of Regnase-1 in the nucleus within 30 minutes (Figure 6A). These results
306 suggest that Regnase-1 dynamically changes its localization between the cytoplasm and the
307 nucleus. Given that Regnase-1 dominantly localizes in the cytoplasm in the steady state
308 conditions, the frequency of its nuclear export seems to be higher than its nuclear import.

309 CRM1 is known to recognize a nuclear export signal (NES) of a cargo protein for the
310 protein export (Hutten & Kehlenbach, 2007). Thus, we investigated if Regnase-1 harbors a
311 NES. *In silico* prediction deduced amino acids 433-447 of Regnase-1 as a potential NES with
312 high probability (Xu et al., 2015) (Figure 6B–D). Indeed, Regnase-1 lacking 422-451
313 spontaneously accumulated in nucleus (Figure 6E). Since NESs are characterized by
314 hydrophobic residues (la Cour et al., 2003), we also inspected which hydrophobic resides of
315 Regnase-1 were important for efficient nuclear export of Regnase-1. We found that L440,
316 M444, L447, and W448 of Regnase-1 were critical for the nuclear export of Regnase-1
317 (Figure 5E). Noteworthy, all the residues are highly conserved among species (Figure 5D).

318 We next examined whether 14-3-3 binding controls the localization of Regnase-1.
319 Interestingly, Regnase-1-ExoSx2 failed to accumulate in the nucleus even after LMB
320 treatment while Regnase-1-WT and -ExoSAAAx2 accumulated in the nucleus by LMB
321 treatment (Figure 6F). This result indicates that Regnase-1-ExoSx2 is unable to translocate
322 into the nucleus like Regnase-1-WT. Taken together, 14-3-3 inhibits the nuclear import of
323 Regnase-1 as well as its binding to target mRNAs.

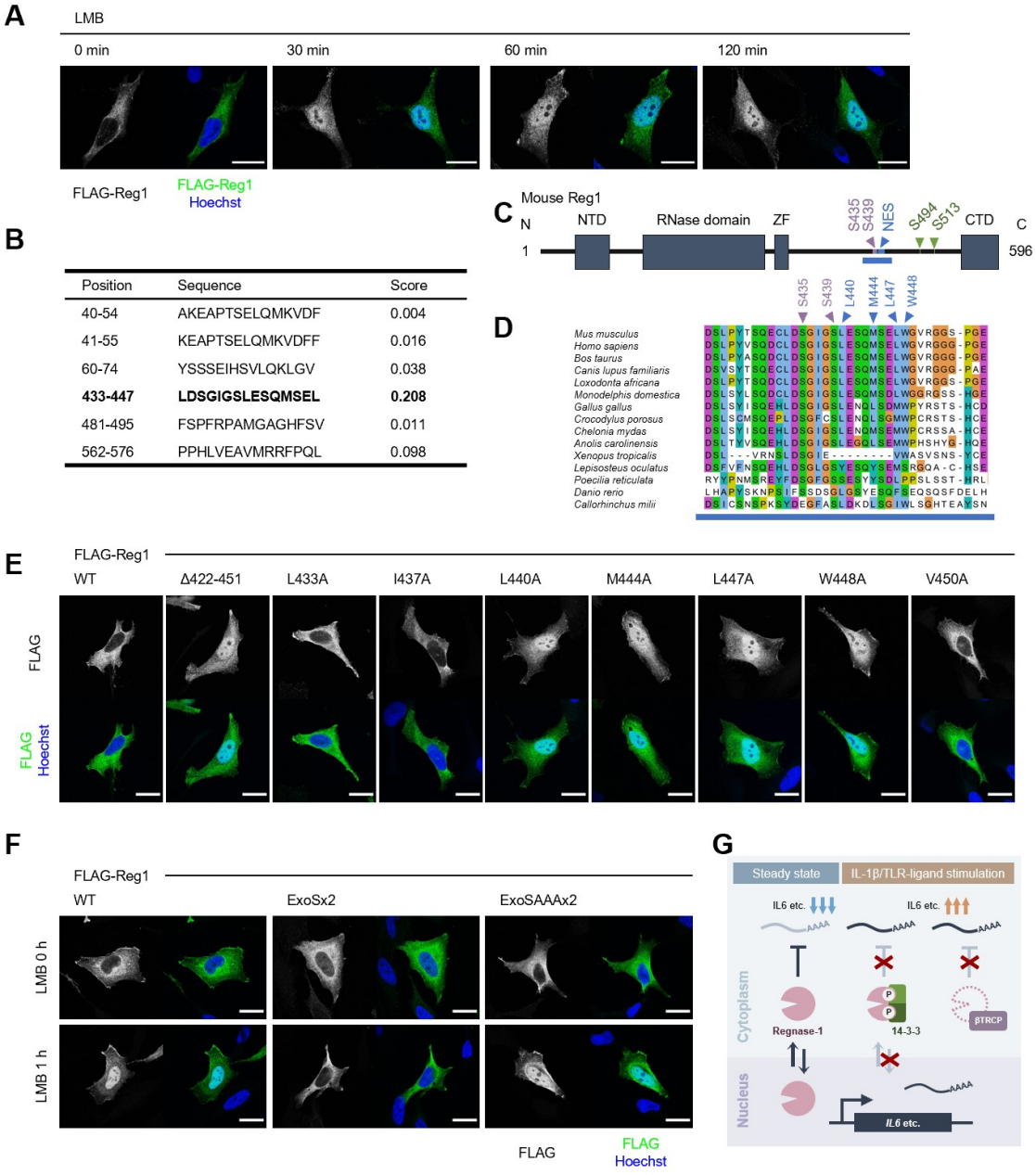

Position	Sequence	Score
40-54	AKEAPTSELQMKVDF	0.004
41-55	KEAPTSELQMKVDFF	0.016
60-74	YSSSEIHSVLQKLGV	0.038
433-447	**LDSGIGSLESQMSEL**	**0.208**
481-495	FSPFRPAMGAGHFSV	0.011
562-576	PPHLVEAVMRRFPQL	0.098

Figure 6 | 14-3-3 inhibit nuclear-cytoplasmic shuttling of Regnase-1.

(**A**) Immunofluorescence analysis of HeLa cells transiently expressing FLAG-Regnase-1-

WT treated with Leptomycin B (LMB) (10 ng/ml) for indicated time. (**B**) The result of NES prediction of Regnase-1 by LocNES. Higher score indicates higher probability. (**C**) Schematic illustration of Regnase-1. The amino acid sequence shown in (D) is highlighted in blue. NTD: N-terminal domain, ZF: Zinc finger domain, CTD: C-terminal domain. (**D**) The amino acid sequences including S435/S439 and NES of Regnase-1 from mouse and other indicated vertebrates. (**E**) Immunofluorescence analysis of HeLa cells transiently expressing FLAG-Regnase-1-WT or indicated mutants. (**F**) Immunofluorescence analysis of HeLa cells transiently expressing FLAG-Regnase-1-WT or indicated mutants treated with LMB (10 ng/ml) for 1 hour. (**G**) Model of 14-3-3 and βTRCP-mediated regulation of Regnase-1. In the steady state, Regnase-1 shuttles between the nucleus and the cytoplasm and degrades target mRNAs such as *Il6*. Under IL-1β or TLR-ligands stimulation, two different regulatory mechanisms suppress the activity of Regnase-1 not to disturb proper expression of inflammatory genes; βTRCP induces protein degradation of Regnase-1 and 14-3-3 inhibits nuclear-cytoplasmic shuttling and mRNA recognition of Regnase-1.

324

Discussion

In the present study, we discovered that IL-1β and TLR stimulation dynamically changes protein-protein interaction of Regnase-1. Particularly, these stimuli trigger the interaction of Regnase-1 with 14-3-3 as well as βTRCP via phosphorylation at distinct amino acids. Whereas phosphorylation of Regnase-1 at S494 and S513 is recognized by 14-3-3, βTRCP associates with Regnase-1 phosphorylated at S435 and S439. We demonstrated that Regnase-1-14-3-3 and Regnase-1-βTRCP binding are not sequential but mutually exclusive events (Figure 3A–B).

14-3-3 and βTRCP inhibit Regnase-1-mediated mRNA decay via distinct mechanisms; 14-3-3 prevents Regnase-1-mRNA binding while βTRCP induces protein degradation of Regnase-1. Analysis of *Regnase-1*$^{S513A/S513A}$ mice revealed that 14-3-3-mediated abrogation of Regnase-1 can be compensated by the degradation of Regnase-1. The presence of this dual regulatory system underscores the importance of restricting the activity of Regnase-1 to ensure proper inflammatory gene expression when cells encounter PAMPs or DAMPs (Figure 6G).

Notably, exome sequence analysis of the colon samples from ulcerative colitis patients discovered mutations in the βTRCP binding site of Regnase-1 (Kakiuchi et al., 2020; Nanki et al., 2020). Furthermore, a previous report showed that *Regnase-1* S435/S439A mutant mice were resistant to experimental autoimmune encephalomyelitis (EAE) (Tanaka et al., 2019). All these mutations abolish βTRCP-mediated degradation of Regnase-1. However, genetic association between the 14-3-3-binding site of Regnase-1 and

346 inflammatory diseases has not been identified so far. This is possibly because of the
347 compensation by βTRCP-mediated regulation, which we observed in *Regnase-1*$^{S513A/S513A}$
348 mice. Previous studies have shown that viral proteins or lncRNAs inhibit βTRCP-mediated
349 protein degradation (Guo et al., 2020; Neidel et al., 2019; van Buuren et al., 2014; Yang et
350 al., 2020). 14-3-3-mediated regulation of Regnase-1 may serve as a backup mechanism to
351 control the activity of Regnase-1 when βTRCP-mediated protein degradation is dysregulated.
352 While βTRCP regulates the abundance of Regnase-1 through protein degradation, 14-
353 3-3 regulates the activity of Regnase-1. We found that 14-3-3-bound Regnase-1 failed to
354 associate with mRNAs, indicating that 14-3-3 prevents Regnase-1 from recognizing target
355 mRNA. We have previously shown that an RNase domain and an adjacent zinc finger domain
356 play an important role in Regnase-1-RNA binding (Yokogawa et al., 2016). However, the 14-
357 3-3-binding site of Regnase-1 is in the C-terminal part of Regnase-1, which is distant from
358 RNase and zinc finger domains. Therefore, 14-3-3 is unlikely to inhibit Regnase-1-mRNA
359 binding by simple competition between 14-3-3 and mRNAs for the RNA binding domain of
360 Regnase-1. We have previously reported that Regnase-1 interacts with CBP80-bound, but not
361 eIF4E-bound, mRNAs, indicating that Regnase-1 recognizes its target mRNA before or
362 immediately after the nuclear export of the mRNA (Mino et al., 2019). In this study, we found
363 that Regnase-1 shuttles between the nucleus and the cytoplasm while 14-3-3-bound Regnase-
364 1 cannot enter the nucleus. Thus, it is tempting to speculate that Regnase-1 recognizes mRNA
365 in the nucleus and induce mRNA decay during pioneer rounds of translation immediately
366 after the nuclear export (Maquat et al., 2010; Müller-Mcnicoll & Neugebauer, 2013).

Nevertheless, further investigation is required to clarify the mechanisms of Regnase-1-mediated mRNA decay depending on its nuclear-cytoplasmic shuttling.

βTRCP is likely to recognize 14-3-3-free Regnase-1, indicating that 14-3-3 inhibits Regnase-1-βTRCP interaction. There are two possible mechanisms to explain this. One posits that 14-3-3 bound to phosphorylated S494 and S513 of Regnase-1 conceals βTRCP-binding site (pS435 and pS439), although the 14-3-3-binding site does not overlap with βTRCP-binding site completely. The other possible explanation is that 14-3-3-mediated inhibition of nuclear-cytoplasmic shuttling of Regnase-1 controls βTRCP-mediated Regnase-1 degradation. Indeed, βTRCP localizes not only in the cytoplasm, but also in the nucleus (Davis et al., 2002). It is plausible that 14-3-3 prevents Regnase-1-βTRCP interaction in the nucleus, by inhibiting nuclear-cytoplasmic shuttling of Regnase-1. Of note, the NES of Regnase-1 is located just adjacent to βTRCP-binding site (Figure 6C–D), implying possibility of competitive binding of βTRCP and CRM1 to Regnase-1.

Among the molecules involved in MyD88-dependent signaling, we found that IRAK1/2 are potent inducers of the interaction between Regnase-1 and 14-3-3, thereby abrogating Regnase-1-mediated mRNA decay. IRAKs are involved in stabilization of inflammatory mRNAs as well as NF-κB activation (Flannery et al., 2011; Hartupee et al., 2008; Wan et al., 2009). A previous study showed that IRAK1-mediated mRNA stabilization does not require IRAK1-TRAF6 association (Hartupee et al., 2008). Interestingly, the IRAK1-TRAF6 association is also dispensable for the Regnase-1-14-3-3 binding. Instead, other evolutionally conserved amino acids in the C-terminal structural domain (CSD) of

IRAK1, R663 and K665, are critical for Regnase-1-14-3-3 binding. Considering 14-3-3-mediated inactivation of Regnase-1, it is plausible that the CSD of IRAK1 is the key for stabilization of inflammatory mRNAs.

In summary, Regnase-1 interactome analysis revealed dynamic 14-3-3-mediated regulation of Regnase-1 in response to IL-1β and TLR stimuli. Since recent studies identified Regnase-1 as a high-potential therapeutic target in various diseases (Kakiuchi et al., 2020; Nanki et al., 2020; Wei et al., 2019), our findings may help maximize the effect of Regnase-1 modulation or provide an alternative way to control the activity of Regnase-1.

Materials and Methods

Mice

Regnase-1-deficient mice have been described previously (Matsushita et al., 2009). *Regnase-1*$^{S513A/S513A}$ knock-in mice were generated using CRISPR/Cas9-mediated genome-editing technology as previously described (Fujihara & Ikawa, 2014). Briefly, a pair of complementary DNA oligos was annealed and inserted into pX330 (Addgene plasmid # 42230) (Cong et al., 2013). The plasmid was injected together with the donor single strand oligo into fertilized eggs of C57BL/6J mice. Successful insertion was confirmed by direct sequencing.

All mice were grown under specific pathogen-free environments. All animal experiments were conducted in compliance with the guidelines of the Kyoto University animal experimentation committee.

Reagents

Recombinant cytokines, TLR ligands, and chemical compounds were listed in the key resources table.

Cell culture

HeLa cells, HEK293T cells, and MEFs were maintained in DMEM (nacalai tesque) with 10 % fetal bovine serum (FBS), 1 % Penicillin/Streptomycin (nacalai tesque), and 100 μM 2-Mercaptoethanol (nacalai tesque).

For the preparation of bone marrow-derived macrophages (BMDMs), bone marrow cells were cultured in RPMI-1640 (nacalai tesque) with 10 % FBS, 1 %

418 Penicillin/Streptomycin, 100 μM 2-mercaptoethanol, and 20 ng/ml of macrophage colony-
419 stimulating factor (M-CSF) (BioLegend) for 6 days.

420 For the preparation of thioglycolate-elicited peritoneal exudate cells (PECs), mice
421 were intraperitoneally injected with 2 ml of 4% (w/v) Brewer's thioglycollate medium. 3.5
422 days after the injection, peritoneal macrophages were collected and cultured in RPMI-1640
423 with 10 % FBS, 1 % Penicillin/Streptomycin, and 100 μM 2-mercaptoethanol.

424 **Plasmids**

425 For the expression of FLAG-tagged proteins, pFLAG-CMV2 (Sigma) was used as a
426 backbone. For the expression of HA- or Myc-tagged proteins, the FLAG sequence of
427 pFLAG-CMV2 was replaced by HA- or Myc-sequence. Mouse Regnase-1 cDNA was
428 inserted into these vectors as previously described (Matsushita et al., 2009). The coding
429 sequences of 14-3-3 and βTRCP were amplified by using cDNAs derived from HeLa cell as
430 templates and inserted into vectors above using In-Fusion HD Cloning Kit (Takara Bio). For
431 Myc-IRAK1 expression vector, coding sequence of IRAK1 derived from HA-IRAK1
432 expression vector (Iwasaki et al., 2011) was used. For the mouse *Il6* expression vector, the
433 EGFP sequence in pEGFP-C1 was replaced with *Il6* gene.

434 Deletions or point mutations were introduced using the QuikChange Lightning Site-
435 Directed Mutagenesis Kit (Agilent) or In-Fusion HD Cloning Kit.

436 For the lentiviral packaging vectors, pInducer20 (Addgene plasmid # 44012)
437 (Meerbrey et al., 2011) was modified to generate pInducer20-puro. FLAG-HA-Regnase-1
438 sequence was inserted into pInducer20-puro using In-Fusion HD Cloning Kit.

Plasmid transfection

Plasmids were transfected to HeLa cells or HEK293T cells using Lipofectamine 2000 (Invitrogen) or PEI max (Polysciences) respectively according to manufacturer's instructions.

Generation of doxycycline-inducible FLAG-HA-Regnase-1-expressing HeLa cells

HeLa cells expressing FLAG-HA-Regnase-1 in a doxycycline-dependent manner were generated by lentiviral transduction. To produce lentivirus, HEK293T cells were transfected with pInducer20-puro-FLAG-HA-Regnase1 together with third generation lentiviral packaging vectors. 6 hours after the transfection, the medium was changed to fresh medium and then the cells were incubated at 37 °C for 48 hours. After the incubation, the medium containing lentivirus was harvested and filtrated through 0.45 μm filter. HeLa cells were incubated with the virus-containing medium at 37 °C for 24 hours, followed by 48-hour-incubation with fresh medium. The transduced cells were selected by 0.5 μg/mL of puromycin (InvivoGen). Single clones were picked and evaluated for their expression of FLAG-HA-Regnase-1 in a dox-dependent manner by immunoblotting.

DSP-crosslinking

Doxycycline-inducible FLAG-HA-Regnase-1-expressing HeLa cells were treated with doxycycline (1 μg/mL, Sigma) and incubated at 37 °C for 4 hours before the DSP-crosslinking. As a negative control, cells were incubated without doxycycline, and for the IL-1β-stimulated sample, cells were stimulated with human IL-1β (10 ng/mL, R&D Systems) 2 hours before the crosslinking. After the incubation, cells were washed twice with pre-warmed PBS, and then incubated in PBS containing 0.1 mM DSP (TCI) at 37 °C for 30 minutes. After

crosslinking, cells were washed once with pre-warmed PBS and incubated in STOP solution (PBS containing 1 M Tris-HCl pH 7.4) at room temperature for 15 minutes. Cells were then washed with ice-cold PBS twice, followed by cell lysis and immunoprecipitation.

Immunoprecipitation

Before immunoprecipitation, pre-washed Dynabeads Protein G (Invitrogen) were incubated with either anti-FLAG antibody (Sigma), anti-HA antibody (Sigma), or anti-Myc antibody (Sigma) at 4 °C with rotation for 1 hour.

For DSP-crosslinked samples, cells were lysed in IP buffer (20 mM Tris-HCl pH 7.4, 150 mM NaCl, and 0.5 % (vol/vol) NP-40) with cOmplete Mini EDTA-free (Sigma), PhosSTOP (Sigma), and 200 U/mL of Benzonase (Millipore) and incubated on ice for 10 minutes. The lysates were centrifuged at 15,000 rpm for 5 minutes and the supernatants were incubated with anti-FLAG-antibody-bound Dynabeads at 4 °C with rotation for 2 hours. The beads were then washed with IP buffer three times and incubated in FLAG-elution buffer (100 μg/mL FLAG peptides (Sigma), 50 mM Tris-HCl pH7.4, and 150 mM NaCl) at 4 °C with rotation for 10 minutes twice. Eluted proteins were then immunoprecipitated using anti-HA-antibody-bound Dynabeads at 4 °C with rotation for 2 hours. After the second immunoprecipitation, the beads were washed three times with IP buffer and the proteins were eluted in Urea elution buffer (8 M Urea and 50 mM Tris-HCl pH 8.0). The samples were stored at -80 °C until trypsin digestion. Proteins were reduced with 10 mM dithiothreitol (Fujifilm Wako) for 30 min, alkylated with 50 mM iodoacetamide (Fujifilm Wako) for 30 min in the dark, diluted 4-fold with 50 mM ammonium bicarbonate (ABC) buffer, and then

481 trypsin digestion was performed. After overnight incubation, digestion was stopped by
482 adding trifluoroacetic acid (TFA) (Fujifilm Wako) to a final concentration of 0.5%. The
483 peptide mixture solution was desalted with SDB-XC StageTips (Rappsilber et al., 2007). The
484 eluates were dried and resuspended in 200 mM 2-[4-2(2-hydroxyethyl)-1-
485 piperazine]ethanesulfonic acid (HEPES) pH 8.5, mixed with 0.1 mg of TMT10-plex labeling
486 reagents (Thermo Fisher Scientific) dissolved in 5 μL acetonitrile (ACN), and incubated for
487 1 h at room temperature. The reaction mixtures were quenched by adding hydroxylamine
488 (Sigma) to give a final concentration of 0.33%. After 15 minutes incubation, the samples
489 were acidified with trifluoroacetic acid, diluted to 5% ACN, and desalted using SDB-XC
490 StageTips. Peptides were dried, resolved in 5 mM ABC buffer and fractionated with a C18-
491 StageTip. Peptides were eluted with 5 mM ABC containing acetonitrile (12.5%, 15%, 17.5%
492 20%, 22.5% and 80%) in step gradient manner. Totally 6 fractions were obtained and
493 analyzed by LC/MS/MS.

494 For the identification of phosphorylation sites of Regnase-1, HeLa cells expressing
495 FLAG-HA-Regnase-1 or FLAG-Regnase-1 were stimulated with IL-1β (10 ng/mL) or IL-
496 17A (50 ng/mL) respectively for 4 hours. The cells were washed with ice-cold PBS twice
497 and lysed in IP buffer with cOmplete Mini EDTA-free and PhosSTOP. Regnase-1 was
498 immunoprecipitated using anti FLAG antibody as described above and eluted from
499 Dynabeads in SDS sample buffer (50 mM Tris–HCl pH 6.8, 2% (wt/vol) SDS, 15% (vol/vol)
500 2-mercaptoethanol, 10% (vol/vol) glycerol and bromophenol blue), followed by incubation
501 at 95°C for 5 minutes. Regnase-1was isolated by electrophoresis and the pieces of the gel

containing Regnase-1 was stored at 4 °C until trypsin digestion. The gels were de-stained for 30 min with 200 µL of 50 mM ABC / 50% ACN. Then the gels were dehydrated by the addition of 100% ACN. Proteins were reduced with 500 µL of 10 mM dithiothreitol / 50 mM ABC for 30 min, alkylated with 50 mM iodoacetamide / 50 mM ABC for 30 min in the dark. The gels were washed two times with 200 µL of 0.5% acetic acid / 50% methanol. After washing, gels were re-equilibrated with 50 mM ABC, and subsequently dehydrated by the addition of 100% ACN. 10 µL of trypsin solution (10 ng/µL in 50 mM ABC) was added to gel pieces and incubated for 5 min. Another 50 µL of 50 mM ABC buffer was added to gel samples and incubated at 37 °C for overnight. After that, elastase (Promega) (150 ng/µL in water) was added to the final concentration of 7.5 ng/µL and incubated for 30 min at 37 °C (Dau et al., 2020). Digestion was stopped by the addition of 5 µL of 10% TFA. The supernatants were recovered into fresh Eppendorf tubes, and two additional extraction steps were performed with 50% ACN / 0.1% TFA and 80% ACN / 0.1% TFA. The peptides in the supernatants were dried, resuspended in 0.1% TFA, and desalted using SDB-XC StageTips.

For detecting protein-protein binding, cells were lysed in IP Buffer with cOmplete Mini EDTA-free and PhosSTOP and immunoprecipitated as described above using indicated antibodies. The proteins were eluted in the mixture of IP Buffer and SDS sample buffer (2:1) and incubated at 95°C for 5 minutes.

For detecting protein-RNA binding, cells were lysed in IP Buffer with cOmplete Mini EDTA-free and RNaseOut (Invitrogen) and immunoprecipitated as described above using indicated antibodies. Some of the precipitates were eluted in the mixture of IP Buffer and

SDS sample buffer (2:1) to elute proteins and the others were eluted in TRIzol Reagent (Invitrogen) for RNA isolation.

LC-MS/MS

LC/MS/MS analyses were performed with an Orbitrap Fusion Lumos (Thermo Fisher Scientific) connected to an Ultimate 3000 pump (Thermo Fisher Scientific) and an HTC-PAL autosampler (CTC analytics). Peptides were separated by a self-pulled needle column (150 mm length, 100 µm ID, 6 µm needle opening) packed with Reprosil-Pur 120 C18-AQ 3 µm reversed-phase material (Dr. Maisch GmbH), using a 20 min or 65 min gradient of 5–40% B (mobile phase A: 0.5% acetic acid, mobile phase B: 0.5% acetic acid / 80% acetonitrile) at a flow rate of 500 nL/min. The applied ESI voltage was 2.4 kV. For TMT labeled samples, the following parameters were applied: MS scan range of 375–1500, MS1 orbitrap resolution of 120,000, quadrupole isolation window of 0.7, HCD (higher-energy collision dissociation) collision energy of 38%, MS2 orbitrap resolution of 50,000, AGC target value of 50000. For non-labeled samples, the following parameters were applied: MS scan range of 300–1500, MS1 orbitrap resolution of 120,000, quadrupole isolation window of 1.6, HCD collision energy of 30%, MS2 orbitrap resolution of 15,000, MS2 AGC target value of 50000.

Database searching and data processing

For DSP-crosslinked samples, peptides were identified with Mascot version 2.6.1 (Matrix Science) against the sequence of Mouse Regnase-1 in addition to the human database from UniprotKB/Swiss-Prot release 2017/04 and with a precursor ion mass tolerance of 5 ppm and a product ion mass tolerance of 20 ppm. Carbamidomethyl (C), TMT6plex (K) and

TMT6plex (N-term) were set as a fixed modification, oxidation (M) was allowed as a variable modification, and up to 2 missed cleavages are allowed with strict Trypsin/P specificity. Identified peptides were rejected if the Mascot score was below the 95% confidence limit based on the identity score of each peptide. The quantification of peptides was based on the TMT reporter ion intensities in MS2 spectra. Protein quantitative values were calculated by summing the corresponding peptide intensity values. Only proteins with at least two unique peptides were used for further analysis.

For the identification of phosphorylation sites of Regnase-1, peptides were identified with Mascot version 2.7.0 against the sequence of mouse Regnase-1 with a precursor ion mass tolerance of 5 ppm and a product ion mass tolerance of 20 ppm. Carbamidomethyl (C) was set as a fixed modification, oxidation (M) and phosphorylation (STY) were allowed as variable modifications, and up to 2 missed cleavages are allowed with semitrypsin specificity. Identified peptides were rejected if the Mascot score was below the 99% confidence limit based on the identity score of each peptide. The label-free quantification of peptides was based on the peak area in the extracted ion chromatograms using Skyline-daily software version 21.0.9.118 (MacLean et al., 2010). The peak area ratios between stimulated and non-stimulated samples were calculated, log-scaled, and normalized by the median. For quantitation of phosphosites, the peak area ratios of all monophosphopeptides containing the phosphosites of interest were averaged. Phosphosite localization was evaluated with a site-determining ion combination method based on the presence of site-determining y- or b-ions in the peak lists of the fragment ions, which supported the phosphosites unambiguously

(Nakagami et al., 2010).

Protein-protein interaction network of the Regnase-1-associating proteins (Log_2 fold change over negative control > 2) was analyzed using STRING database (Szklarczyk et al., 2019) and visualized in Cytoscape (Shannon et al., 2003). Keratins contaminated in the samples were omitted from the analysis.

RNA isolation and RT-qPCR

Cells were lysed in TRIzol Reagent, and the RNA was isolated according to manufacturer's instructions. For the isolation of the RNA precipitated with Regnase-1, RNA was isolated using RNA Clean & Concentrator-5 (Zymo Research). RNA was reverse transcribed by using ReverTra Ace (TOYOBO). cDNA was amplified by using PowerUp SYBR Green Master Mix (Applied Biosystems) and measured with StepOnePlus Real-Time PCR System (Applied Biosystems). To analyze mRNA expression, each RNA level was normalized with 18S or ACTB. The primers used in qPCR were listed in Supplementary Table.

RNA Sequencing

PECs were harvested from *Regnase-1*$^{WT/WT}$ and *Regnase-1*$^{S513A/S513A}$ mice as described above. PECs were stimulated with LPS (100 ng/ml) for indicated time and the RNA was collected and isolated using TRIzol Reagent. cDNA library was prepared using NEBNext Ultra RNA Library Prep Kit for Illumina (NEB) and sequenced on NextSeq 500 System (Illumina) according to the manufacturer’s instructions. Acquired data was analyzed using Galaxy (Afgan et al., 2018). Briefly, identified reads were mapped on the murine genome (mm10) using HISAT2 (paired end, unstranded) (Galaxy Version 2.1.0), and the mapped

586 reads were counted using featureCounts (Galaxy Version 1.6.3).

587 **Data availability**

588 Mass spectrometry data have been deposited to the ProteomeXchange Consortium
589 (http://proteomecentral.proteomexchange.org) via the jPOST partner repository (Moriya et
590 al., 2019; Okuda et al., 2017) (http://jpostdb.org) with the data set identifier PXD026561.

591 RNA sequencing data have been deposited to GEO (Accession code: GSE180028).

592 **Immunoblotting**

593 Cells were lysed in IP Buffer or RIPA buffer (1% (vol/vol) NP-40, 0.1% (wt/vol) SDS, 1%
594 (wt/vol) sodium deoxycholate, 150 mM NaCl, 20 mM Tris-HCl pH 8.0, and 10 mM EDTA)
595 with cOmplete Mini EDTA-free and PhosSTOP. The lysates were incubated on ice for 5
596 minutes and centrifuged at 15,000 rpm for 5 minutes. The supernatants were mixed with SDS
597 sample buffer (2:1) and incubated at 95°C for 5 minutes. SDS-PAGE was performed using
598 e-PAGEL 7.5% or 5~20% (ATTO) and the proteins were transferred onto 0.2 μm pore size
599 Immun-Blot PVDF membranes (Bio-Rad), followed by blocking with 5 % skim milk. The
600 antibodies used in immunoblotting were listed in the key resources table. Luminescence was
601 detected with Amersham Imager 600 (cytiva) and the images were analyzed with Fiji
602 (Schindelin et al., 2012).

603 **λ-protein phosphatase (λPP) treatment**

604 HeLa cells transiently expressing HA-14-3-3ε were stimulated with or without IL-1β (10
605 ng/mL) for 4 hours and lysed in IP Buffer. Some of the lysates were used in
606 immunoprecipitation as described above. The proteins were eluted using 250 μg/mL of HA

607 peptides as described above. The lysate and the precipitates were treated with Lambda
608 Protein Phosphatase (NEB) according to manufacturer's instructions. For the λPP negative
609 samples, the same amount of IP Buffer was added instead of λPP.

610 **ELISA**

611 Cytokine concentration was measured by using IL-6 Mouse Uncoated ELISA Kit
612 (Invitrogen) according to manufacturer's instructions. Luminescence was detected with
613 iMark Microplate Reader (Bio-Rad).

614 **Luciferase assay**

615 5xNF-κB firefly luciferase reporter vector, Renilla luciferase vector, and IRAK1-expressing
616 vector were transfected in HeLa cells and the luciferase activity was measured by using
617 PicaGene Dual Sea Pansy Luminescence Kit (TOYO B-Net). NF-κB activation was
618 calculated by normalizing Firefly luciferase activity with Renilla luciferase activity.

619 **Mathematical model**

620 We developed two dynamical models for the inflammation system regulated by Regnase-1
621 based on different assumptions of the functions of 14-3-3-bound Regnase-1.

622

623 **Model 1**

624 In the first model, we assumed that the 14-3-3-bound Regnase-1 does not have the function
625 of degrading its target mRNAs (Figure 4J). The ordinary differential equations are given as
626 follows:

$$\begin{aligned}\frac{dx_1}{dt} &= k_1 signal(t) - d_1 x_1 x_3 - d_4 x_1 \\ \frac{dx_2}{dt} &= k_2 signal(t) - d_2 x_2 x_3 - d_5 x_2 \\ \frac{dx_3}{dt} &= k_3 x_2 - (d_3 + d_6 signal(t) + d_7 signal(t)) x_3 + d_9 x_4 \\ \frac{dx_4}{dt} &= d_7 signal(t) x_3 - (d_8 + d_9) x_4\end{aligned} \tag{1.1}$$

where x_1, x_2, x_3, and x_4 is the abundance of *Il6* mRNA, *Reg1* mRNA, Reg1 Protein, and 14-3-3-bound Reg1 Protein, respectively; k_1 and k_2 is the transcription rate constant of *Il6*, and *Reg1*, respectively; k_3 is the translation rate constant of *Reg1*; d_1 and d_2 is the Reg1-induced degradation rate constant of *Il6* mRNA and *Reg1* mRNA, respectively; d_3, d_4, and d_5 is the Reg1-independent degradation rate constant of Reg1 protein, *Il6* mRNA, and *Reg1* mRNA, respectively; d_6 is the ubiquitin-dependent degradation rate constant of Reg1 protein; d_7 is the binding rate constant of Reg1 protein to 14-3-3; d_8 is the natural degradation rate constant of 14-3-3-bound Reg1 protein; d_9 is the dissociation rate constant of Reg1 from 14-3-3. $signal(t)$ is the strength of TLR stimulation, which is given as the following form (Mino et al., 2019):

$$signal(t) = \begin{cases} s_{base} \ (if\ 0 \le t \le t_{delay}), \\ \frac{s_{input} - s_{base}}{t_{raise}}(t - t_{delay}) + s_{base} \ (if\ t_{delay} \le t \le t_{delay} + t_{raise}), \\ s_{input} \ (if\ t_{delay} + t_{raise} \le t \le t_{delay} + t_{raise} + t_{pulse}), \\ (s_{input} - s_{base}) \times \exp\left(-\frac{t - (t_{delay} + t_{raise} + t_{pulse})}{t_{delay}}\right) + s_{input} \\ (if\ t > t_{delay} + t_{raise} + t_{pulse}) \end{cases} \tag{1.2}$$

638 **Model 2**

639 We also developed an alternative model in which the 14-3-3-bound Regnase-1 maintains
640 functions of degrading its target mRNAs (Figure 4J). The ordinary differential equations
641 are given as follows:

$$\begin{aligned}
\frac{\mathrm{d}\hat{x}_1}{\mathrm{d}t} &= k_1 signal(t) - d_1\hat{x}_1\hat{x}_3 - d_1{}'\,\hat{x}_1\hat{x}_4 - d_4\hat{x}_1 \\
\frac{\mathrm{d}\hat{x}_2}{\mathrm{d}t} &= k_2 signal(t) - d_2\hat{x}_2\hat{x}_3 - d_2{}'\,\hat{x}_2\hat{x}_4 - d_5 x_2 \\
\frac{\mathrm{d}\hat{x}_3}{\mathrm{d}t} &= k_3 x_2 - (d_3 + d_6 signal(t) + d_7 signal(t))\hat{x}_3 + d_9\hat{x}_4 \\
\frac{\mathrm{d}\hat{x}_4}{\mathrm{d}t} &= d_7 signal(t)\hat{x}_3 - (d_8 + d_9)\hat{x}_4
\end{aligned} \tag{1.3}$$

642 where $\hat{x}_1$, $\hat{x}_2$, $\hat{x}_3$, and $\hat{x}_4$ is the abundance of *Il6* mRNA, *Reg1* mRNA, Reg1 Protein, 14-
643 3-3-bound Reg1 Protein, respectively; $d_1{}'$ and $d_2{}'$ is the 14-3-3-bound Reg1-induced
644 degradation rate constant of *Il6* mRNA and *Reg1* mRNA, respectively. The other
645 parameters are defined in the same way as Model 1.

646 To determine which model is consistent with the experimental observations, we
647 focus on the experimental findings that there was no difference in the abundance of *Il*6
648 mRNA, *Reg1* mRNA, and Reg1- protein (without 14-3-3 bound) between *Regnase-1*$^{WT/WT}$
649 and *Regnase-1*$^{S513A/S513A}$ cells in the late phase of stimulation (Figure 4A, B, D, and E). We
650 will show that in Model 2 (1.3), the abundance of the *Il6* mRNAs should be different
651 between *Regnase-1*$^{WT/WT}$ and *Regnase-1*$^{S513A/S513A}$ cells under the condition that amount of
652 the 14-3-3-free Reg1 protein is comparable between them.

653

654 **Analysis of the equilibrium**

655 Lemma 1. For *Regnase-1*$^{WT/WT}$ cells, there exists only one nonnegative (biologically

656 meaningful) equilibrium of the system (1.3) if and only if $d_3 + d_6 s_{input} + d_7 s_{input} -$

657 $\frac{d_7 d_9 s_{input}}{d_7 s_{input} + d_9} \geq 0$. If $d_3 + d_6 s_{input} + d_7 s_{input} - \frac{d_7 d_9 s_{input}}{d_7 s_{input} + d_9} < 0$, there is no equilibrium.

658 For *Regnase-1*$^{S513A/S513A}$ cells, there always exists only one nonnegative (biologically

659 meaningful) equilibrium.

660 Proof of lemma 1:

661 Setting all the derivatives of (1.3) equal to zero yields

$$\begin{aligned} 0 &= k_1 s_{input} - d_1 \hat{X}_1^{WT} \hat{X}_3^{WT} - d_1{}' \hat{X}_1^{WT} \hat{X}_4^{WT} - d_4 \hat{X}_1^{WT} \\ 0 &= k_2 s_{input} - d_2 \hat{X}_2^{WT} \hat{X}_3^{WT} - d_2{}' \hat{X}_2^{WT} \hat{X}_4^{WT} - d_5 \hat{X}_2^{WT} \\ 0 &= k_3 \hat{X}_2^{WT} - (d_3 + d_6 s_{input} + d_7 s_{input}) \hat{X}_3^{WT} + d_9 \hat{X}_4^{WT} \\ 0 &= d_7 s_{input} \hat{X}_3^{WT} - (d_8 + d_9) \hat{X}_4^{WT} \end{aligned} \tag{1.4}$$

662 where $\hat{X}_1^{WT}$, $\hat{X}_2^{WT}$, $\hat{X}_3^{WT}$, and $\hat{X}_4^{WT}$ are fixed points of $\hat{x}_1$, $\hat{x}_2$, $\hat{x}_3$, and $\hat{x}_4$, respectively.

663 Given that $signal(t) \to s_{input}$ as $t \to \infty$, we assume $signal(t) \approx s_{input}$ at the

664 equilibrium.

665 It follows from (1.4) that

$$\left(d_2 + \frac{d_7 s_{input}}{d_8 + d_9} d_2{}'\right) K (\hat{X}_3^{WT})^2 + d_5 K \hat{X}_3^{WT} - k_2 s_{input} = 0 \tag{1.5a}$$

666

$$\hat{X}_4^{WT} = \frac{d_7 s_{input}}{d_8 + d_9} \hat{X}_3^{WT} \tag{1.5b}$$

667

$$\hat{X}_2^{WT} = K \hat{X}_3^{WT} \tag{1.5c}$$

668

$$\hat{X}_1^{WT} = \frac{k_1 s_{input}}{d_1 \hat{X}_3^{WT} + d_1{}' \hat{X}_4^{WT} + d_4} \tag{1.5d}$$

669 where

670 $$K := \frac{1}{k_3}\left(d_3 + d_6 s_{input} + d_7 s_{input} - \frac{d_7 d_9 s_{input}}{d_7 s_{input} + d_9} \right)$$

671 It is easy to see that the quadratic equation (1.5a) has a nonnegative solution if $K \geq 0$, i.e.

672 $d_3 + d_6 s_{input} + d_7 s_{input} - \frac{d_7 d_9 s_{input}}{d_7 s_{input} + d_9} \geq 0$. If $K < 0$, (1.5a) has no nonnegative solution. If

673 $\hat{X}_3^{WT} \geq 0$, it follows from (1.5b), (1.5c), and (1.5d) that $\hat{X}_4^{WT}$, $\hat{X}_2^{WT}$, $\hat{X}_1^{WT} \geq 0$.

674

675 For *Regnase-1*$^{S513A/S513A}$ cells, we assume that $d_7 = d_8 = d_9 = 0$. Substituting this

676 equation into (1.4) yields

$$\begin{aligned} 0 &= k_1 s_{input} - d_1 \hat{X}_1^{SA} \hat{X}_3^{SA} - d_4 \hat{X}_1^{SA} \\ 0 &= k_2 s_{input} - d_2 \hat{X}_2^{SA} \hat{X}_3^{SA} - d_5 \hat{X}_2^{SA} \\ 0 &= k_3 \hat{X}_2^{SA} - (d_3 + d_6 s_{input}) \hat{X}_3^{SA} \\ 0 &= \hat{X}_4^{SA} \end{aligned} \tag{1.6}$$

677 where $\hat{X}_1^{SA}$, $\hat{X}_2^{SA}$, $\hat{X}_3^{SA}$, and $\hat{X}_4^{SA}$ are fixed points of $\hat{x}_1$, $\hat{x}_2$, $\hat{x}_3$, and $\hat{x}_4$ in *Regnase-*

678 $I^{S513A/S513A}$ cells, respectively.

679 It follows from (1.6) that

$$d_2 \frac{k_3}{d_3 + d_6 s_{input}} (\hat{X}_2^{SA})^2 + d_5 \hat{X}_2^{SA} - k_2 s_{input} = 0 \quad (1.7a)$$

680

$$\hat{X}_3^{SA} = \frac{k_3}{d_3 + d_6 s_{input}} \hat{X}_2^{SA} \quad (1.7b)$$

681

$$\hat{X}_1^{SA} = \frac{k_1 s_{input}}{d_1 \hat{X}_3^{SA} + d_4} \quad (1.7c)$$

682 It is easy to see that the quadratic equation (1.7a) has a nonnegative solution. If $\hat{X}_2^{SA} \geq 0$, it

683 follows from (1.7b) and (1.7c) that $\hat{X}_3^{SA}$ $\hat{X}_1^{SA} \geq 0$.

684

685 Lemma 2. There exists only one nonnegative (biologically meaningful) equilibrium of the

686 system (1.1) if and only if $d_3 + d_6 s_{input} + d_7 s_{input} - \frac{d_7 d_9 s_{input}}{d_7 s_{input} + d_9} \geq 0$. If $d_3 +$

687 $d_6 s_{input} + d_7 s_{input} - \frac{d_7 d_9 s_{input}}{d_7 s_{input} + d_9} < 0$, there is no equilibrium. For *Regnase-1*$^{S513A/S513A}$

688 cells, there always exists only one nonnegative (biologically meaningful) equilibrium.

689 Proof of lemma2:

690 With $d_1' = d_2' = 0$ in lemma 1, we get the same conclusion.

691

692 **Consistency with the experiments**

693 The experimental observation shows that there was no difference in the abundance of Reg1
694 protein between *Regnase-1*$^{WT/WT}$ and *Regnase-1*$^{S513A/S513A}$ cells at the late phase of
695 stimulation (Figure 4A–C), which implies

$$\hat{X}_3^{WT} \approx \hat{X}_3^{SA} \tag{1.8}$$

696 , based on the alternative model (1.3).

697

698 From (1.4) and (1.6), we get

$$\begin{aligned} \hat{X}_1^{WT} &= \frac{k_1 s_{input}}{d_1 \hat{X}_3^{WT} + d_1{}' \hat{X}_4^{WT} + d_4} \\ \hat{X}_2^{WT} &= \frac{k_2 s_{input}}{d_2 \hat{X}_3^{WT} + d_2{}' \hat{X}_4^{WT} + d_5} \end{aligned} \tag{1.9a}$$

699

$$\begin{aligned} \hat{X}_1^{SA} &= \frac{k_1 s_{input}}{d_1 \hat{X}_3^{SA} + d_4} \\ \hat{X}_2^{SA} &= \frac{k_2 s_{input}}{d_2 \hat{X}_3^{SA} + d_5} \end{aligned} \tag{1.9b}$$

700 By (1.8), (1.9a), and (1.9b), we obtain

$$\hat{X}_1^{WT} < \hat{X}_1^{SA} \tag{1.10a}$$

701

$$\hat{X}_2^{WT} < \hat{X}_2^{SA} \tag{1.10b}$$

702 (1.10a) and (1.10b) implies that in Model 2, the abundance of *Il6* and *Regnase-1* mRNA in
703 *Regnase-1*$^{WT/WT}$ cells should be smaller than that in *Regnase-1*$^{S513A/S513A}$ cells at the late

704 phase under the condition that amount of the Reg1 protein is comparable (1.8) between
705 these two cells. It contradicts experimental observation that the abundance of the *Il6* and
706 *Regnase-1* mRNAs did not differ between *Regnase-1*$^{WT/WT}$ and *Regnase-1*$^{S513A/S513A}$ cells
707 (Figure 4D-I). Thus, Model 2 (1.3) is not consistent with the experimental findings.
708 In contrast, in Model 1 (1.1), we assume from experimental findings that

$$X_3^{WT} \approx X_3^{SA} \tag{1.11}$$

709 , just like (1.8), where X_3^{WT} is the fixed point of x_3 in *Regnase-1*$^{WT/WT}$ cells and X_3^{SA} is the
710 fixed point of x_3 in *Regnase-1*$^{S513A/S513A}$ cells based on the model (1.1).
711 By substituting $d_7 = d_8 = d_9 = 0$ into (1.9a) and (1.9b), we obtain

$$X_1^{WT} = \frac{k_1 s_{input}}{d_1 X_3^{WT} + d_4}$$
$$X_2^{WT} = \frac{k_2 s_{input}}{d_2 X_3^{WT} + d_5} \tag{1.12a}$$

712

$$X_1^{SA} = \frac{k_1 s_{input}}{d_1 X_3^{SA} + d_4}$$
$$X_2^{SA} = \frac{k_2 s_{input}}{d_2 X_3^{SA} + d_5} \tag{1.12b}$$

713 where X_1^{WT} and X_2^{WT} are fixed points of x_1 and x_2, respectively in *Regnase-1*$^{WT/WT}$ cells
714 and X_1^{SA} and X_2^{SA} are fixed points of x_1 and x_2, respectively in *Regnase-1*$^{S513A/S513A}$ cells.
715 By (1.11), (1.12a), and (1.12b), we obtain

$$X_1^{WT} \approx X_1^{SA} \tag{1.13a}$$

716

$$X_2^{WT} \approx X_2^{SA} \quad (1.13b)$$

717 In this case, (1.13a) and (1.13b) are in agreement with the experimental facts that that the
718 abundance of the target mRNAs did not differ between *Regnase-1*$^{WT/WT}$ and *Regnase-*
719 *1*$^{S513A/S513A}$ cells.

720 These mathematical analyses indicate that Model 1 (1.1), but not Model 2 (1.3), is
721 consistent with the experimental findings.

722

723 **Immunofluorescence**

724 Cells were cultured on cover glass, fixed with 4%-Paraformaldehyde Phosphate Buffer
725 Solution (nacalai tesque), and permeabilized with 0.5 % (vol/vol) Triton X-100 (nacalai
726 tesque) in PBS, followed by incubation in blocking solution (2 % (vol/vol) goat serum
727 (FUJIFILM Wako Pure Chemical) and 0.1 % (wt/vol) gelatin in PBS). The antibodies used
728 in Immunofluorescence were listed in the key resources table. DNA was stained with Hoechst
729 33342 (Invitrogen). Fluorescence was detected with TCS SPE (Leica). Acquired images were
730 analyzed with Fiji (Schindelin et al., 2012).

731 **Amino acid sequence analysis**

732 Amino acid sequence of each protein was obtained from NCBI. The results of T-coffee
733 alignment (Notredame et al., 2000) were visualized by using Jalview (Waterhouse et al.,
734 2009). Secondary structure was predicted by using PSIPRED 4.0 (Buchan & Jones, 2019;
735 Jones, 1999). NES prediction was performed by using LocNES (Xu et al., 2015).

Acknowledgements

We thank S. Ogawa and N. Kakiuchi in Kyoto university for performing RNA sequencing, Y. Okumoto for secretarial assistance and lab members for helpful discussion. This work was supported by Japan Society for the Promotion of Science (JSPS) KAKENHI [18H05278]; AMED-FORCE [JP20gm4010002] from Japan Agency for Medical Research and Development and the JSPS through Core-to-Core Program. K.A. was supported by "Kibou Projects" Scholarship for doctoral Students in Immunology. T.M. was funded by JSPS KAKENHI (19H03488), Grant-in-Aid for Scientific Research on Innovative Areas "Genome Science" (221S0002 and 16H06279), Takeda Science Foundation, the Uehara Memorial Foundation, Shimizu Foundation for Immunology and Neuroscience, Naito Foundation, Senri Life Science Foundation, Nakajima Foundation, and Mochida Memorial Foundation for Medical and Pharmaceutical Research.

748 **References**

749 Afgan, E., Baker, D., Batut, B., Van Den Beek, M., Bouvier, D., Ech, M., Chilton, J.,
750 Clements, D., Coraor, N., Grüning, B. A., Guerler, A., Hillman-Jackson, J.,
751 Hiltemann, S., Jalili, V., Rasche, H., Soranzo, N., Goecks, J., Taylor, J., Nekrutenko,
752 A., & Blankenberg, D. (2018). The Galaxy platform for accessible, reproducible and
753 collaborative biomedical analyses: 2018 update. *Nucleic Acids Research*, *46*(W1),
754 W537–W544. https://doi.org/10.1093/nar/gky379

755 Aitken, A. (2006). 14-3-3 proteins: A historic overview. *Seminars in Cancer Biology*,
756 *16*(3), 162–172. https://doi.org/10.1016/j.semcancer.2006.03.005

757 Akira, S., Uematsu, S., & Takeuchi, O. (2006). Pathogen recognition and innate immunity.
758 *Cell*, *124*(4), 783–801. https://doi.org/10.1016/j.cell.2006.02.015

759 Anderson, P. (2010). Post-transcriptional regulons coordinate the initiation and resolution
760 of inflammation. *Nature Reviews Immunology*, *10*(1), 24–35.
761 https://doi.org/10.1038/nri2685

762 Buchan, D. W. A., & Jones, D. T. (2019). The PSIPRED Protein Analysis Workbench: 20
763 years on. *Nucleic Acids Research*, *47*(W1), W402–W407.
764 https://doi.org/10.1093/nar/gkz297

765 Carpenter, S., Ricci, E. P., Mercier, B. C., Moore, M. J., & Fitzgerald, K. A. (2014). Post-
766 transcriptional regulation of gene expression in innate immunity. *Nature Reviews*
767 *Immunology*, *14*(6), 361–376. https://doi.org/10.1038/nri3682

768 Cong, L., Ran, F. A., Cox, D., Lin, S., Barretto, R., Habib, N., Hsu, P. D., Wu, X., Jiang,

769 W., Marraffini, L. A., & Zhang, F. (2013). Multiplex genome engineering using
770 CRISPR/Cas systems. *Science*, *339*(6121), 819–823.
771 https://doi.org/10.1126/science.1231143
772 Dau, T., Bartolomucci, G., & Rappsilber, J. (2020). Proteomics Using Protease Alternatives
773 to Trypsin Benefits from Sequential Digestion with Trypsin. *Analytical Chemistry*,
774 *92*(14), 9523–9527. https://doi.org/10.1021/acs.analchem.0c00478
775 Davis, M., Hatzubai, A., Andersen, J. S., Ben-Shushan, E., Fisher, G. Z., Yaron, A.,
776 Bauskin, A., Mercurio, F., Mann, M., & Ben-Neriah, Y. (2002). Pseudosubstrate
777 regulation of the SCFβ-TrCP ubiquitin ligase by hnRNP-U. *Genes and Development*,
778 *16*(4), 439–451. https://doi.org/10.1101/gad.218702
779 Fitzgerald, K. A., & Kagan, J. C. (2020). Toll-like Receptors and the Control of Immunity.
780 *Cell*, *180*(6), 1044–1066. https://doi.org/10.1016/j.cell.2020.02.041
781 Flannery, S. M., Keating, S. E., Szymak, J., & Bowie, A. G. (2011). Human interleukin-1
782 receptor-associated kinase-2 is essential for toll-like receptor-mediated transcriptional
783 and post-transcriptional regulation of tumor necrosis factor α. *Journal of Biological*
784 *Chemistry*, *286*(27), 23688–23697. https://doi.org/10.1074/jbc.M111.248351
785 Fu, H., Coburn, J., & Collier, R. J. (1993). The eukaryotic host factor that activates
786 exoenzyme S of Pseudomonas aeruginosa is a member of the 14-3-3 protein family.
787 *Proceedings of the National Academy of Sciences of the United States of America*,
788 *90*(6), 2320–2324. https://doi.org/10.1073/pnas.90.6.2320
789 Fujihara, Y., & Ikawa, M. (2014). CRISPR/Cas9-based genome editing in mice by single

790 plasmid injection. In *Methods in Enzymology* (Vol. 546, Issue C, pp. 319–336).
791 Academic Press Inc. https://doi.org/10.1016/B978-0-12-801185-0.00015-5
792 Gottipati, S., Rao, N. L., & Fung-Leung, W. P. (2008). IRAK1: A critical signaling
793 mediator of innate immunity. *Cellular Signalling*, *20*(2), 269–276.
794 https://doi.org/10.1016/j.cellsig.2007.08.009
795 Guo, C. J., Ma, X. K., Xing, Y. H., Zheng, C. C., Xu, Y. F., Shan, L., Zhang, J., Wang, S.,
796 Wang, Y., Carmichael, G. G., Yang, L., & Chen, L. L. (2020). Distinct Processing of
797 lncRNAs Contributes to Non-conserved Functions in Stem Cells. *Cell*, *181*(3), 621-
798 636.e22. https://doi.org/10.1016/j.cell.2020.03.006
799 Hao, S., & Baltimore, D. (2009). The stability of mRNA influences the temporal order of
800 the induction of genes encoding inflammatory molecules. *Nature Immunology*, *10*(3),
801 281–288. https://doi.org/10.1038/ni.1699
802 Hartupee, J., Li, X., & Hamilton, T. (2008). Interleukin 1α-induced NFκB activation and
803 chemokine mRNA stabilization diverge at IRAK. *Journal of Biological Chemistry*,
804 *283*(23), 15689–15693. https://doi.org/10.1074/jbc.M801346200
805 Hutten, S., & Kehlenbach, R. H. (2007). CRM1-mediated nuclear export: to the pore and
806 beyond. *Trends in Cell Biology*, *17*(4), 193–201.
807 https://doi.org/10.1016/j.tcb.2007.02.003
808 Iwasaki, H., Takeuchi, O., Teraguchi, S., Matsushita, K., Uehata, T., Kuniyoshi, K., Satoh,
809 T., Saitoh, T., Matsushita, M., Standley, D. M., & Akira, S. (2011). The IκB kinase
810 complex regulates the stability of cytokine-encoding mRNA induced by TLR–IL-1R

by controlling degradation of regnase-1. *Nature Immunology*, *12*(12), 1167–1175. https://doi.org/10.1038/ni.2137

Jones, D. T. (1999). Protein secondary structure prediction based on position-specific scoring matrices. *Journal of Molecular Biology*, *292*(2), 195–202. https://doi.org/10.1006/jmbi.1999.3091

Kakiuchi, N., Yoshida, K., Uchino, M., Kihara, T., Akaki, K., Inoue, Y., Kawada, K., Nagayama, S., Yokoyama, A., Yamamoto, S., Matsuura, M., Horimatsu, T., Hirano, T., Goto, N., Takeuchi, Y., Ochi, Y., Shiozawa, Y., Kogure, Y., Watatani, Y., … Ogawa, S. (2020). Frequent mutations that converge on the NFKBIZ pathway in ulcerative colitis. *Nature*, *577*(7789), 260–265. https://doi.org/10.1038/s41586-019-1856-1

Karlberg, T., Hornyak, P., Pinto, A. F., Milanova, S., Ebrahimi, M., Lindberg, M., Püllen, N., Nordström, A., Löverli, E., Caraballo, R., Wong, E. V., Näreoja, K., Thorsell, A. G., Elofsson, M., De La Cruz, E. M., Björkegren, C., & Schüler, H. (2018). 14-3-3 proteins activate Pseudomonas exotoxins-S and -T by chaperoning a hydrophobic surface. *Nature Communications*, *9*(1), 1–11. https://doi.org/10.1038/s41467-018-06194-1

Kollewe, C., Mackensen, A. C., Neumann, D., Knop, J., Cao, P., Li, S., Wesche, H., & Martin, M. U. (2004). Sequential Autophosphorylation Steps in the Interleukin-1 Receptor-associated Kinase-1 Regulate its Availability as an Adapter in Interleukin-1 Signaling. *Journal of Biological Chemistry*, *279*(7), 5227–5236.

https://doi.org/10.1074/jbc.M309251200

la Cour, T., Gupta, R., Rapacki, K., Skriver, K., Poulsen, F. M., & Brunak, S. (2003). NESbase version 1.0: A database of nuclear export signals. *Nucleic Acids Research*, *31*(1), 393–396. https://doi.org/10.1093/nar/gkg101

MacLean, B., Tomazela, D. M., Shulman, N., Chambers, M., Finney, G. L., Frewen, B., Kern, R., Tabb, D. L., Liebler, D. C., & MacCoss, M. J. (2010). Skyline: An open source document editor for creating and analyzing targeted proteomics experiments. *Bioinformatics*, *26*(7), 966–968. https://doi.org/10.1093/bioinformatics/btq054

Maquat, L. E., Tarn, W. Y., & Isken, O. (2010). The pioneer round of translation: Features and functions. *Cell*, *142*(3), 368–374. https://doi.org/10.1016/j.cell.2010.07.022

Masters, S. C., Pederson, K. J., Zhang, L., Barbieri, J. T., & Fu, H. (1999). Interaction of 14-3-3 with a nonphosphorylated protein ligand, exoenzyme S of Pseudomonas aeruginosa. *Biochemistry*, *38*(16), 5216–5221. https://doi.org/10.1021/bi982492m

Matsushita, K., Takeuchi, O., Standley, D. M., Kumagai, Y., Kawagoe, T., Miyake, T., Satoh, T., Kato, H., Tsujimura, T., Nakamura, H., & Akira, S. (2009). Zc3h12a is an RNase essential for controlling immune responses by regulating mRNA decay. *Nature*, *458*(7242), 1185–1190. https://doi.org/10.1038/nature07924

Meerbrey, K. L., Hu, G., Kessler, J. D., Roarty, K., Li, M. Z., Fang, J. E., Herschkowitz, J. I., Burrows, A. E., Ciccia, A., Sun, T., Schmitt, E. M., Bernardi, R. J., Fu, X., Bland, C. S., Cooper, T. A., Schiff, R., Rosen, J. M., Westbrook, T. F., & Elledge, S. J. (2011). The pINDUCER lentiviral toolkit for inducible RNA interference in vitro and

in vivo. *Proceedings of the National Academy of Sciences of the United States of America*, *108*(9), 3665–3670. https://doi.org/10.1073/pnas.1019736108

Mino, T., Iwai, N., Endo, M., Inoue, K., Akaki, K., Hia, F., Uehata, T., Emura, T., Hidaka, K., Suzuki, Y., Standley, D. M., Okada-Hatakeyama, M., Ohno, S., Sugiyama, H., Yamashita, A., & Takeuchi, O. (2019). Translation-dependent unwinding of stem–loops by UPF1 licenses Regnase-1 to degrade inflammatory mRNAs. *Nucleic Acids Research*. https://doi.org/10.1093/nar/gkz628

Mino, T., Murakawa, Y., Fukao, A., Vandenbon, A., Wessels, H. H., Ori, D., Uehata, T., Tartey, S., Akira, S., Suzuki, Y., Vinuesa, C. G., Ohler, U., Standley, D. M., Landthaler, M., Fujiwara, T., & Takeuchi, O. (2015). Regnase-1 and roquin regulate a common element in inflammatory mRNAs by spatiotemporally distinct mechanisms. *Cell*, *161*(5), 1058–1073. https://doi.org/10.1016/j.cell.2015.04.029

Moriya, Y., Kawano, S., Okuda, S., Watanabe, Y., Matsumoto, M., Takami, T., Kobayashi, D., Yamanouchi, Y., Araki, N., Yoshizawa, A. C., Tabata, T., Iwasaki, M., Sugiyama, N., Tanaka, S., Goto, S., & Ishihama, Y. (2019). The jpost environment: An integrated proteomics data repository and database. *Nucleic Acids Research*, *47*(D1), D1218–D1224. https://doi.org/10.1093/nar/gky899

Müller-Mcnicoll, M., & Neugebauer, K. M. (2013). How cells get the message: Dynamic assembly and function of mRNA-protein complexes. *Nature Reviews Genetics*, *14*(4), 275–287. https://doi.org/10.1038/nrg3434

Muslin, A. J., Tanner, J. W., Allen, P. M., & Shaw, A. S. (1996). Interaction of 14-3-3 with

874 signaling proteins is mediated by the recognition of phosphoserine. *Cell*, *84*(6), 889–
875 897. https://doi.org/10.1016/S0092-8674(00)81067-3
876 Nakagami, H., Sugiyama, N., Mochida, K., Daudi, A., Yoshida, Y., Toyoda, T., Tomita,
877 M., Ishihama, Y., & Shirasu, K. (2010). Large-scale comparative phosphoproteomics
878 identifies conserved phosphorylation sites in plants. *Plant Physiology*, *153*(3), 1161–
879 1174. https://doi.org/10.1104/pp.110.157347
880 Nanki, K., Fujii, M., Shimokawa, M., Matano, M., Nishikori, S., Date, S., Takano, A.,
881 Toshimitsu, K., Ohta, Y., Takahashi, S., Sugimoto, S., Ishimaru, K., Kawasaki, K.,
882 Nagai, Y., Ishii, R., Yoshida, K., Sasaki, N., Hibi, T., Ishihara, S., … Sato, T. (2020).
883 Somatic inflammatory gene mutations in human ulcerative colitis epithelium. *254* |
884 *Nature* |, *577*. https://doi.org/10.1038/s41586-019-1844-5
885 Neidel, S., Ren, H., Torres, A. A., & Smith, G. L. (2019). NF-κB activation is a turn on for
886 vaccinia virus phosphoprotein A49 to turn off NF-κB activation. *Proceedings of the*
887 *National Academy of Sciences of the United States of America*, *116*(12), 5699–5704.
888 https://doi.org/10.1073/pnas.1813504116
889 Notredame, C., Higgins, D. G., & Heringa, J. (2000). T-coffee: A novel method for fast and
890 accurate multiple sequence alignment. *Journal of Molecular Biology*, *302*(1), 205–
891 217. https://doi.org/10.1006/jmbi.2000.4042
892 O'Neill, L. A. J., Golenbock, D., & Bowie, A. G. (2013). The history of Toll-like receptors-
893 redefining innate immunity. *Nature Reviews Immunology*, *13*(6), 453–460.
894 https://doi.org/10.1038/nri3446

Okuda, S., Watanabe, Y., Moriya, Y., Kawano, S., Yamamoto, T., Matsumoto, M., Takami, T., Kobayashi, D., Araki, N., Yoshizawa, A. C., Tabata, T., Sugiyama, N., Goto, S., & Ishihama, Y. (2017). JPOSTrepo: An international standard data repository for proteomes. *Nucleic Acids Research*, *45*(D1), D1107–D1111. https://doi.org/10.1093/nar/gkw1080

Ottmann, C., Yasmin, L., Weyand, M., Veesenmeyer, J. L., Diaz, M. H., Palmer, R. H., Francis, M. S., Hauser, A. R., Wittinghofer, A., & Hallberg, B. (2007). Phosphorylation-independent interaction between 14-3-3 and exoenzyme S: From structure to pathogenesis. *EMBO Journal*, *26*(3), 902–913. https://doi.org/10.1038/sj.emboj.7601530

Pennington, K. L., Chan, T. Y., Torres, • Mp, & Andersen, • Jl. (2018). The dynamic and stress-adaptive signaling hub of 14-3-3: emerging mechanisms of regulation and context-dependent protein-protein interactions. *Oncogene*, *37*, 5587–5604. https://doi.org/10.1038/s41388-018-0348-3

Rappsilber, J., Mann, M., & Ishihama, Y. (2007). Protocol for micro-purification, enrichment, pre-fractionation and storage of peptides for proteomics using StageTips. *Nature Protocols*, *2*(8), 1896–1906. https://doi.org/10.1038/nprot.2007.261

Schindelin, J., Arganda-Carreras, I., Frise, E., Kaynig, V., Longair, M., Pietzsch, T., Preibisch, S., Rueden, C., Saalfeld, S., Schmid, B., Tinevez, J. Y., White, D. J., Hartenstein, V., Eliceiri, K., Tomancak, P., & Cardona, A. (2012). Fiji: An open-source platform for biological-image analysis. *Nature Methods*, *9*(7), 676–682.

916 https://doi.org/10.1038/nmeth.2019

917 Shannon, P., Markiel, A., Ozier, O., Baliga, N. S., Wang, J. T., Ramage, D., Amin, N.,

918 Schwikowski, B., & Ideker, T. (2003). Cytoscape: A software Environment for

919 integrated models of biomolecular interaction networks. *Genome Research*, *13*(11),

920 2498–2504. https://doi.org/10.1101/gr.1239303

921 Szklarczyk, D., Gable, A. L., Lyon, D., Junge, A., Wyder, S., Huerta-Cepas, J., Simonovic,

922 M., Doncheva, N. T., Morris, J. H., Bork, P., Jensen, L. J., & Von Mering, C. (2019).

923 STRING v11: Protein-protein association networks with increased coverage,

924 supporting functional discovery in genome-wide experimental datasets. *Nucleic Acids*

925 *Research*, *47*(D1), D607–D613. https://doi.org/10.1093/nar/gky1131

926 Takeuchi, O., & Akira, S. (2010). Pattern Recognition Receptors and Inflammation. *Cell*,

927 *140*(6), 805–820. https://doi.org/10.1016/j.cell.2010.01.022

928 Tanaka, H., Arima, Y., Kamimura, D., Tanaka, Y., Takahashi, N., Uehata, T., Maeda, K.,

929 Satoh, T., Murakami, M., & Akira, S. (2019). Phosphorylation-dependent Regnase-1

930 release from endoplasmic reticulum is critical in IL-17 response. *Journal of*

931 *Experimental Medicine*, *216*(6). https://doi.org/10.1084/jem.20181078

932 Turner, M., & DÍaz-Muñoz, M. D. (2018). RNA-binding proteins control gene expression

933 and cell fate in the immune system review-article. In *Nature Immunology* (Vol. 19,

934 Issue 2, pp. 120–129). Nature Publishing Group. https://doi.org/10.1038/s41590-017-

935 0028-4

936 Uehata, T., Iwasaki, H., Vandenbon, A., Matsushita, K., Hernandez-Cuellar, E., Kuniyoshi,

K., Satoh, T., Mino, T., Suzuki, Y., Standley, D. M., Tsujimura, T., Rakugi, H., Isaka, Y., Takeuchi, O., & Akira, S. (2013). Malt1-induced cleavage of regnase-1 in CD4(+) helper T cells regulates immune activation. *Cell*, *153*(5), 1036–1049. https://doi.org/10.1016/j.cell.2013.04.034

van Buuren, N., Burles, K., Schriewer, J., Mehta, N., Parker, S., Buller, R. M., & Barry, M. (2014). EVM005: An Ectromelia-Encoded Protein with Dual Roles in NF-κB Inhibition and Virulence. *PLoS Pathogens*, *10*(8), 1004326. https://doi.org/10.1371/journal.ppat.1004326

Verdoodt, B., Benzinger, A., Popowicz, G. M., Holak, T. A., & Hermeking, H. (2006). Characterization of 14-3-3sigma dimerization determinants: Requirement of homodimerization for inhibition of cell proliferation. *Cell Cycle*, *5*(24), 2920–2926. https://doi.org/10.4161/cc.5.24.3571

Wan, Y., Xiao, H., Affolter, J., Kim, T. W., Bulek, K., Chaudhuri, S., Carlson, D., Hamilton, T., Mazumder, B., Stark, G. R., Thomas, J., & Li, X. (2009). Interleukin-1 receptor-associated kinase 2 is critical for lipopolysaccharide-mediated post-transcriptional control. *Journal of Biological Chemistry*, *284*(16), 10367–10375. https://doi.org/10.1074/jbc.M807822200

Waterhouse, A. M., Procter, J. B., Martin, D. M. A., Clamp, M., & Barton, G. J. (2009). Jalview Version 2-A multiple sequence alignment editor and analysis workbench. *Bioinformatics*, *25*(9), 1189–1191. https://doi.org/10.1093/bioinformatics/btp033

Wei, J., Long, L., Zheng, W., Dhungana, Y., Lim, S. A., Guy, C., Wang, Y., Wang, Y. D.,

Qian, C., Xu, B., Kc, A., Saravia, J., Huang, H., Yu, J., Doench, J. G., Geiger, T. L., & Chi, H. (2019). Targeting REGNASE-1 programs long-lived effector T cells for cancer therapy. *Nature*, *576*(7787), 471–476. https://doi.org/10.1038/s41586-019-1821-z

Wesche, H., Henzel, W. J., Shillinglaw, W., Li, S., & Cao, Z. (1997). MyD88: An adapter that recruits IRAK to the IL-1 receptor complex. *Immunity*, *7*(6), 837–847. https://doi.org/10.1016/S1074-7613(00)80402-1

Xu, D., Marquis, K., Pei, J., Fu, S. C., Całatay, T., Grishin, N. V., & Chook, Y. M. (2015). LocNES: A computational tool for locating classical NESs in CRM1 cargo proteins. *Bioinformatics*, *31*(9), 1357–1365. https://doi.org/10.1093/bioinformatics/btu826

Yaffe, M. B., Rittinger, K., Volinia, S., Caron, P. R., Aitken, A., Leffers, H., Gamblin, S. J., Smerdon, S. J., & Cantley, L. C. (1997). The structural basis for 14-3-3:phosphopeptide binding specificity. *Cell*, *91*(7), 961–971. https://doi.org/10.1016/S0092-8674(00)80487-0

Yang, Q., Li, K., Huang, X., Zhao, C., Mei, Y., Li, X., Jiao, L., & Yang, H. (2020). lncRNA SLC7A11-AS1 Promotes Chemoresistance by Blocking SCFβ-TRCP-Mediated Degradation of NRF2 in Pancreatic Cancer. *Molecular Therapy - Nucleic Acids*, *19*, 974–985. https://doi.org/10.1016/j.omtn.2019.11.035

Yashiroda, Y., & Yoshida, M. (2005). Nucleo-Cytoplasmic Transport of Proteins as a Target for Therapeutic Drugs. *Current Medicinal Chemistry*, *10*(9), 741–748. https://doi.org/10.2174/0929867033457791

979 Yasmin, L., Jansson, A. L., Panahandeh, T., Palmer, R. H., Francis, M. S., & Hallberg, B.
980 (2006). Delineation of exoenzyme S residues that mediate the interaction with 14-3-3
981 and its biological activity. *FEBS Journal*, *273*(3), 638–646.
982 https://doi.org/10.1111/j.1742-4658.2005.05100.x
983 Ye, H., Arron, J. R., Lamothe, B., Cirilli, M., Kobayashi, T., Shevde, N. K., Segal, D.,
984 Dzivenu, O. K., Vologodskaia, M., Yim, M., Du, K., Singh, S., Pike, J. W., Darnay, B.
985 G., Choi, Y., & Wu, H. (2002). Distinct molecular mechanism for initiating TRAF6
986 signalling. *Nature*, *418*(6896), 443–447. https://doi.org/10.1038/nature00888
987 Yokogawa, M., Tsushima, T., Noda, N. N., Kumeta, H., Enokizono, Y., Yamashita, K.,
988 Standley, D. M., Takeuchi, O., Akira, S., & Inagaki, F. (2016). Structural basis for the
989 regulation of enzymatic activity of Regnase-1 by domain-domain interactions.
990 *Scientific Reports*, *6*, 22324. https://doi.org/10.1038/srep22324

Figure Legends (Figure Supplements)

Figure 1—figure supplement 1

Regnase-1 binds to 14-3-3β/γ/ε/ζ/η/θ but not 14-3-3σ

Immunoblot analysis of immunoprecipitates (IP: HA) and WCL from HeLa cells transiently expressing HA-14-3-3β, γ, ε, ζ, η, θ, or σ stimulated with IL-1β (10 ng/ml) for 4 hours.

Figure 2—figure supplement 1

Regnase-1 bands migrate slower in LPS-stimulated samples

Immunoblot analysis of *Regnase-1*$^{WT/WT}$ and *Regnase-1*$^{-/-}$ thioglycollate-elicited PECs stimulated with LPS (100 ng/ml) for indicated time.

Figure 2—figure supplement 2

Candidate spectra of Regnase-1 phosphopeptides with confident site localization.

Only quantitatively altered phosphopeptides are shown. Fragment ions containing the N-(b-type ions) or C-(y-type ions) terminus are labeled with red (without neutral loss) or orange (with neutral-loss).

Figure 2—figure supplement 3

Schematic illustration of IRAK1

The result of secondary structure prediction is shown below. DD: Death domain, CSD: C-terminal structural domain.

Figure 2—figure supplement 4

R663/K665A mutation does not abrogate IRAK1-mediated NF-κB activation

Luciferase activity of HeLa cells transiently transfected with NF-κB luciferase reporter plasmid together with expression plasmids of IRAK1-WT or indicated mutants.

Figure 2—figure supplement 5

IL-17A stimulation induces phosphorylation at S494 and S513 of Regnase-1

Quantitation of phosphosites on Regnase-1 in HeLa cells stimulated with or without IL-17A (50 ng/ml) for 4 hours. Each dot shows phosphosite quantitative ratio between IL-17A+ and IL-17A-. Phosphosites with $\log_2$ ratio > 1 were colored with red. Black horizontal line shows Regnase-1 protein quantitative ratio derived from the average of non-phosphopeptide quantitative ratios, and its error bars show the standard deviation.

Figure 2—figure supplement 6

Candidate spectra of Regnase-1 phosphopeptides with confident site localization

Only quantitatively altered phosphopeptides are shown. Fragment ions containing the N-(b-type ions) or C-(y-type ions) terminus are labeled with red (without neutral loss) or orange (with neutral-loss).

Figure 2—figure supplement 7

IL-17A stimulation induces Regnase-1-14-3-3 association

Immunoblot analysis of immunoprecipitates (IP: HA) and WCL from HeLa cells transiently expressing HA-14-3-3γ and FLAG-Regnase-1-WT or indicated mutants stimulated with IL-17A (50 ng/ml) for 4 hours.

Figure 4—figure supplement 1

Schematic illustration of *Regnase-1* gene in mice

The result of Sanger sequencing around S513 of Regnase-1 are shown below.

Figure 4—figure supplement 2

Il6 expression in *Regnase-1*$^{-/-}$ PECs

mRNA expression of *Il6* and *Regnase-1* in *Regnase-1*$^{WT/WT}$ and *Regnase-1*$^{-/-}$ thioglycollate-elicited PECs stimulated with LPS (100 ng/ml) for indicated time.

Bars represent mean values of biological replicates (n = 3), and error bars represent standard deviation.

Figure 4—figure supplement 3

S513A mutation of Regnase-1 does not affect gene expression

Transcriptome analysis of *Regnase-1*$^{WT/WT}$ and *Regnase-1*$^{S513A/S513A}$ thioglycollate-elicited PECs stimulated with LPS (100 ng/ml) for indicated time. Several known Regnase-1 target transcripts are annotated. None of transcripts shows significant (adjusted p value < 0.05) difference between *Regnase-1*$^{WT/WT}$ and *Regnase-1*$^{S513A/S513A}$.

Figure 5—figure supplement 1

Regnase-1-ExoSx2-D141N binds to 14-3-3

Immunoblot analysis of immunoprecipitates (IP: FLAG) and WCL from HeLa cells transiently expressing FLAG-Regnase-1-D141N or indicated mutants. L.C.: light chain.

Source Data Files

Raw data of the results of immunoblotting are zipped in Source Data Files.

Figure 1—figure supplement 1

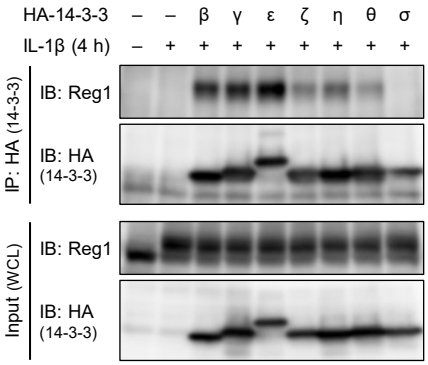

Regnase-1 binds to 14-3-3β/γ/ε/ζ/η/θ but not 14-3-3σ

Immunoblot analysis of immunoprecipitates (IP: HA) and WCL from HeLa cells transiently expressing HA-14-3-3β, γ, ε, ζ, η, θ, or σ stimulated with IL-1β (10 ng/ml) for 4 hours.

Figure 2—figure supplement 1

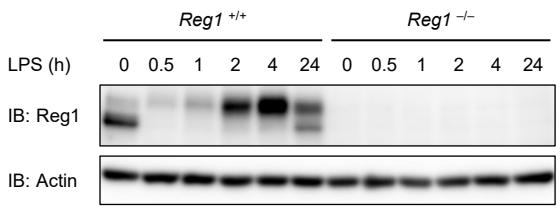

Regnase-1 bands migrate slower in LPS-stimulated samples
Immunoblot analysis of *Regnase-1*$^{WT/WT}$ and *Regnase-1*$^{-/-}$ thioglycollate-elicited PECs stimulated with LPS (100 ng/ml) for indicated time.

Figure 2—figure supplement 2

Phosphosite: S494, Mascot ion score: 118

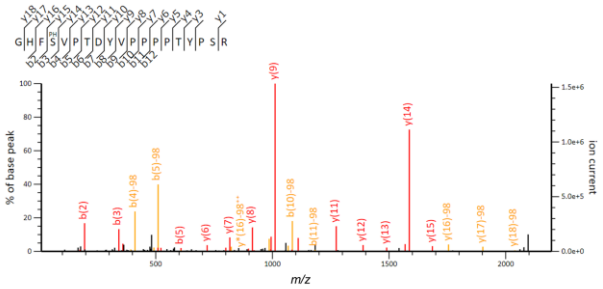

Phosphosite : S62, Mascot ion score : 58

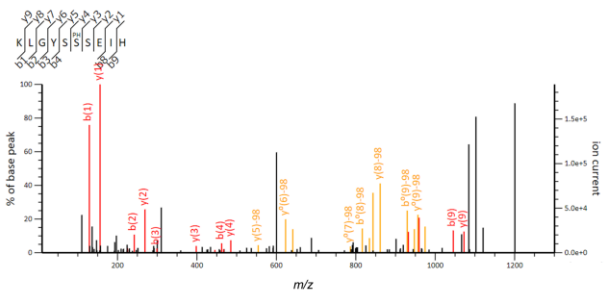

Phosphosite : S513, Mascot ion score : 44

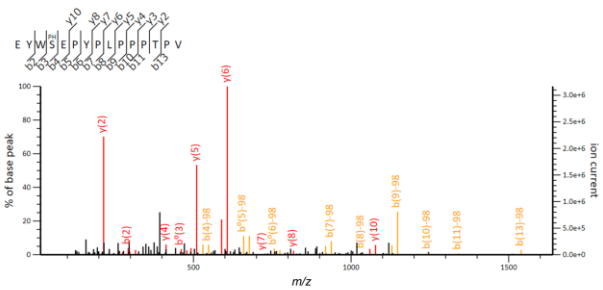

Phosphosite: S61, Mascot ion score : 56

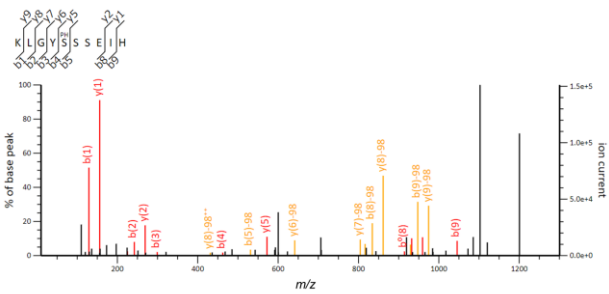

Phosphosite: S362, Mascot ion score : 53

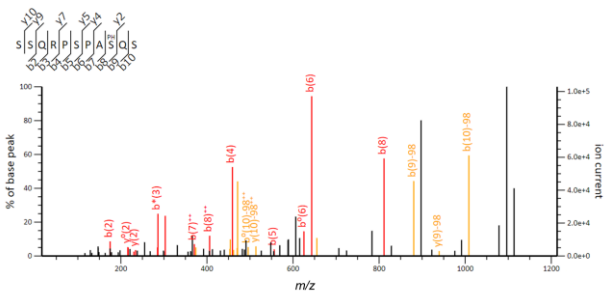

Phosphosite: S439, Mascot ion score : 88

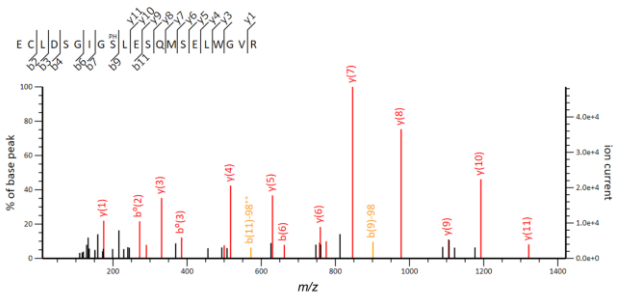

Phosphosite: S470, Mascot ion score : 41

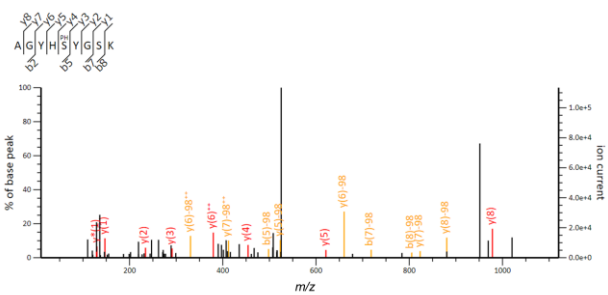

Phosphosite: S21, Mascot ion score : 35

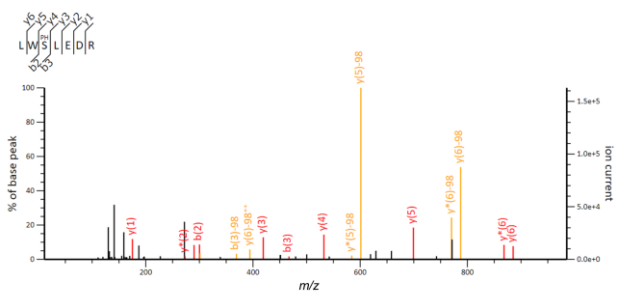

Candidate spectra of Regnase-1 phosphopeptides with confident site localization.
Only quantitatively altered phosphopeptides are shown. Fragment ions containing the N-(b-type ions) or C-(y-type ions) terminus are labeled with red (without neutral loss) or orange (with neutral-loss).

Figure 2—figure supplement 3

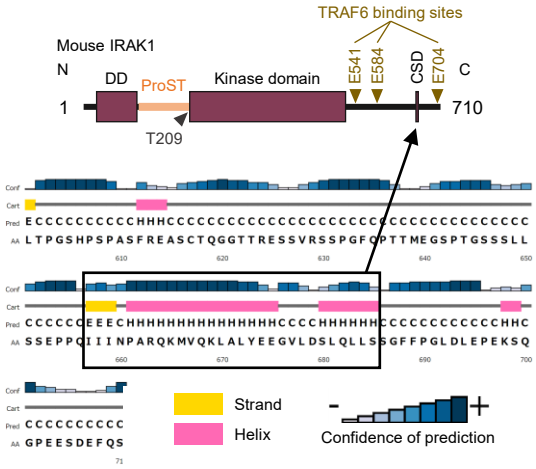

Schematic illustration of IRAK1
The result of secondary structure prediction is shown below. DD: Death domain, CSD: C-terminal structural domain.

Figure 2—figure supplement 4

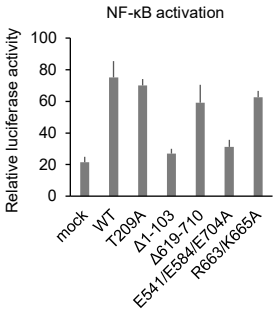

R663/K665A mutation does not abrogate IRAK1-mediated NF-κB activation
Luciferase activity of HeLa cells transiently transfected with NF-κB luciferase reporter plasmid together with expression plasmids of IRAK1-WT or indicated mutants.

Figure 2—figure supplement 5

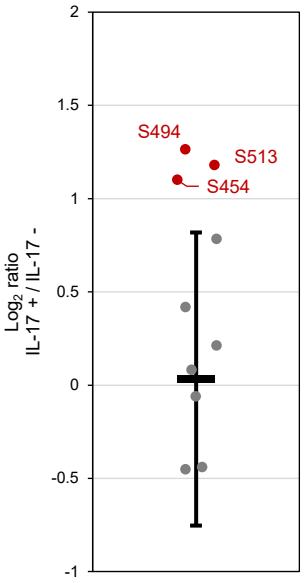

IL-17A stimulation induces phosphorylation at S494 and S513 of Regnase-1

Quantitation of phosphosites on Regnase-1 in HeLa cells stimulated with or without IL-17A (50 ng/ml) for 4 hours. Each dot shows phosphosite quantitative ratio between IL-17A+ and IL-17A-. Phosphosites with $\log_2$ ratio > 1 were colored with red. Black horizontal line shows Regnase-1 protein quantitative ratio derived from the average of non-phosphopeptide quantitative ratios, and its error bars show the standard deviation.

Figure 2—figure supplement 6

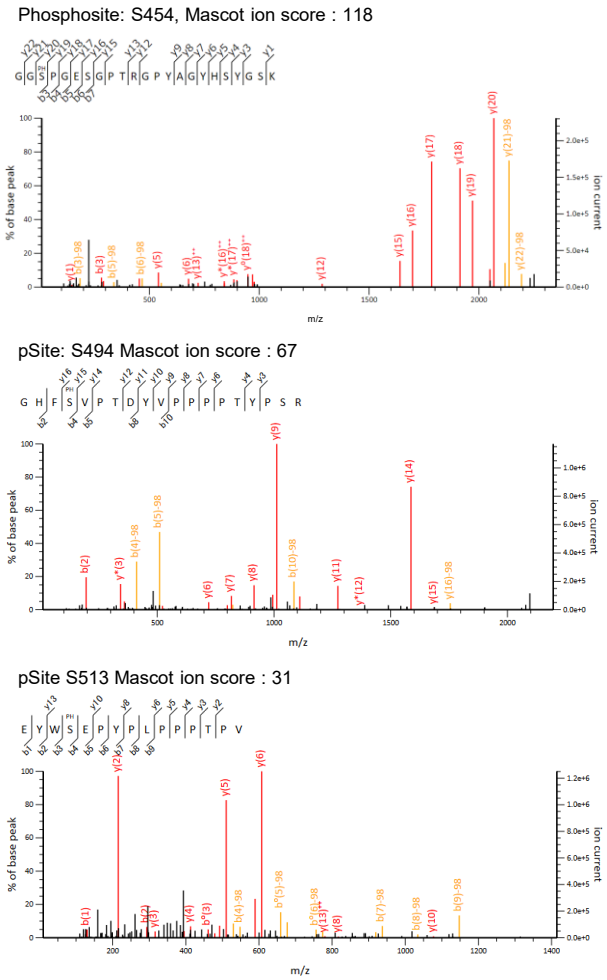

Candidate spectra of Regnase-1 phosphopeptides with confident site localization

Only quantitatively altered phosphopeptides are shown. Fragment ions containing the N-(b-type ions) or C-(y-type ions) terminus are labeled with red (without neutral loss) or orange (with neutral-loss).

Figure 2—figure supplement 7

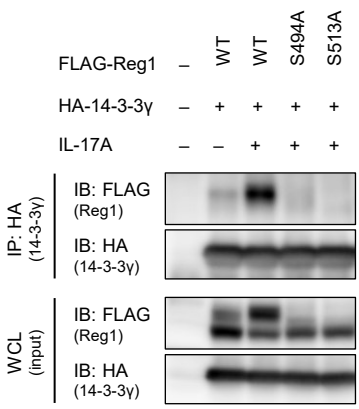

IL-17A stimulation induces Regnase-1-14-3-3 association

Immunoblot analysis of immunoprecipitates (IP: HA) and WCL from HeLa cells transiently expressing HA-14-3-3γ and FLAG-Regnase-1-WT or indicated mutants stimulated with IL-17A (50 ng/ml) for 4 hours.

Figure 4—figure supplement 1

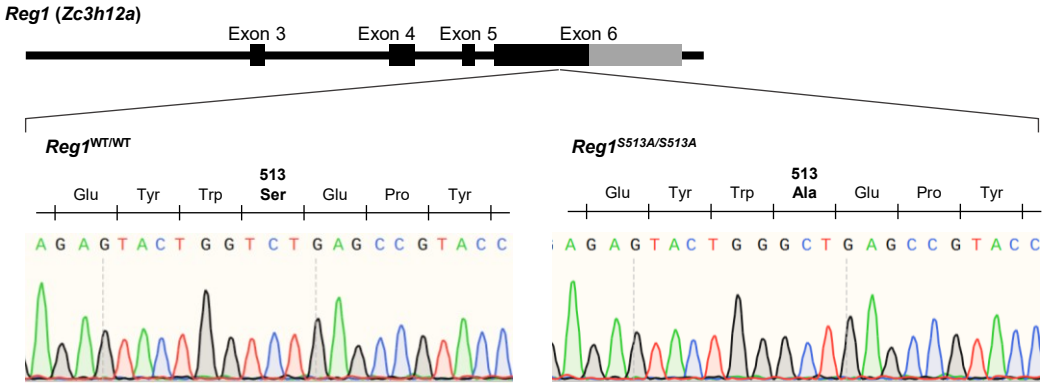

Schematic illustration of *Regnase-1* gene in mice
The result of Sanger sequencing around S513 of Regnase-1 are shown below.

Figure 4—figure supplement 2

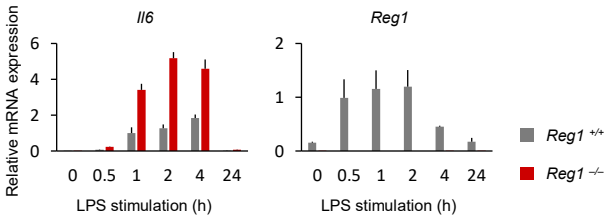

Il6 expression in *Regnase-1*$^{-/-}$ PECs
mRNA expression of *Il6* and *Regnase-1* in *Regnase-1*$^{WT/WT}$ and *Regnase-1*$^{-/-}$ thioglycollate-elicited PECs stimulated with LPS (100 ng/ml) for indicated time.
Bars represent mean values of biological replicates (n = 3), and error bars represent standard deviation.

Figure 4—figure supplement 3

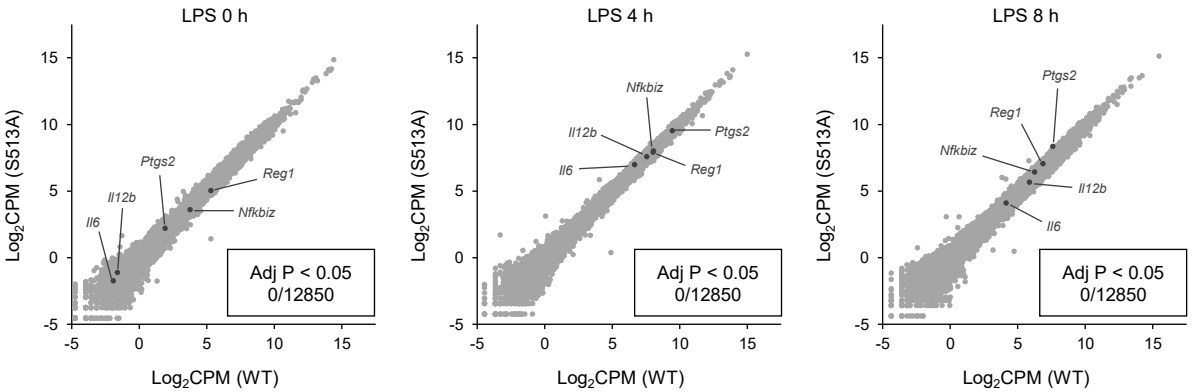

S513A mutation of Regnase-1 does not affect gene expression
Transcriptome analysis of *Regnase-1*$^{WT/WT}$ and *Regnase-1*$^{S513A/S513A}$ thioglycollate-elicited PECs stimulated with LPS (100 ng/ml) for indicated time. Several known Regnase-1 target transcripts are annotated. None of transcripts shows significant (adjusted p value < 0.05) difference between *Regnase-1*$^{WT/WT}$ and *Regnase-1*$^{S513A/S513A}$.

Figure 5—figure supplement 1

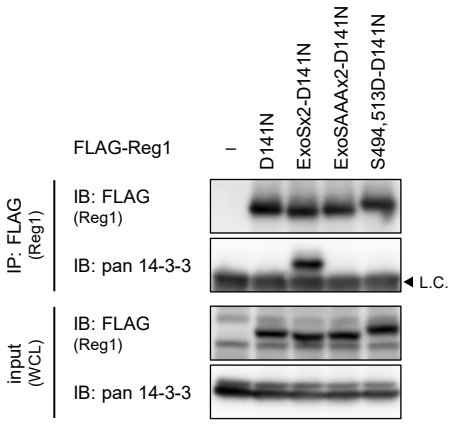

Regnase-1-ExoSx2-D141N binds to 14-3-3

Immunoblot analysis of immunoprecipitates (IP: FLAG) and WCL from HeLa cells transiently expressing FLAG-Regnase-1-D141N or indicated mutants. L.C.: light chain.